NASA Contractor Report 159232

EARTH RADIATION BUDGET MEASUREMENTS FROM SATELLITES AND THEIR INTERPRETATION FOR CLIMATE MODELING AND STUDIES

Thomas H. Vonder Haar, Principal Investigator

Research Institute of Colorado
Fort Collins, CO 80526

CONTRACT NAS1-15553
APRIL, 1980

National Aeronautics and
Space Administration

Langley Research Center
Hampton, Virginia 23665
AC 804 827-3966

ABSTRACT

This paper presents the annual and seasonal averaged earth atmosphere radiation budgets derived from the most complete set of satellite observations available in late 1979. The budgets are derived from a composite of 48 monthly mean radiation budget maps. The annual, global average emitted infrared flux is 234 $W.m^{-2}$, planetary albedo is 0.30 and the net flux is zero within measurement uncertainty. The influence of continentality is apparent in the geographic distribution of the radiation budget, particularly planetary albedo. The net flux distributions display distinct regions of zonal asymetry particularly within those regions (latitudes) associated with the maximum solar insolation.

The globally averaged net flux displays an annual cycle which is mainly attributed to the annual cycle imposed by external forcings associated with regular variation of the solar declination throughout the year. A study of the geographical distribution of the total variability of the net flux reveals that generally greater than 95% of the variability occurs as a result of the semi and annual cycles forced by external earth-sun variations. However, the amounts of energy contained in the variance unexplained by these cycles is vast. Thus, we direct radiation modeling studies to these regions and situations where the potential for climate change impact due to radiation budget variability is the greatest. The individual components of emitted flux and planetary albedo display expectedly more high frequency variability particularly equatorward of 30^{o} latitude governed by weather disturbances and their attendant cloud distributions.

Radiative transfer model simulations of the observed budget quantities at the "top-of-the-atmosphere" are good at least for the zonally averaged case. Significant differences exist between the present surface radiation budget calculations to those previously estimated. The differences, largely a result of the exclusion of enhanced absorption in the window region (8-14 μm) by earlier budget calculations, provide some 35 $W.m^{-2}$ more radiant energy into the oceans in the tropics than previously estimated. The validity of this result was verified using GATE radiation budget measurements. The results of the radiation budget measurements imply that it may be difficult and ambiguous to verify radiative transfer calculations of climate models using satellite observations without consideration of the surface situation. The net radiation flux, and particularly its variation, can be generally modelled successfully in terms of simple earth-sun geometry requirements with seasonally invariant cloud cover. However, this does not ensure that either the surface budgets or the atmospheric heating are modelled adequately. Neither does it insure that areas of non-reciprocity in radiation exchange with space; areas of potentially high climatic impact are properly represented by the general treatment.

1. Introduction

The earth's radiation balance has been a subject of a number of studies for many years. Crucial to the question of climate research is the knowledge of the solar radiation input and the longwave radiation output at the top of the atmosphere and the exchange of heat, momentum and material (especially water vapour) at the bottom. Furthermore, it is necessary to know the size and scale of interannual variations in the components of the energy budget. It is particularly important to assess the role of oceans in climatic variations and the extent and variability of the partitioning of the heat transport between the atmosphere and the oceans. It is evident that accurate and extensive measurements of the earth's radiation budget are required particularly over a period of several years to provide insight as to the extent of the interannual variabilities. Satellite measurements presently provide the best estimate of the earth radiation budget with sufficient temporal and spatial resolution over the entire globe. Further, from a combination of such data with conventional measurements of atmospheric and oceanic variables, the heat transports within the ocean and atmosphere can be deduced (e.g. Oort and Vonder Haar, 1976).

A number of studies have been presented over the last 10-15 years regarding the mean steady state magnitudes of the energy exchange between earth and space. For example, Vonder Haar and Suomi (1969, 1971) presented results for the mean annual and seasonal cases based on measurements during five years (1962-1966). Others, including Winston (1967) and Raschke and Bandeen (1970) discussed short spans of data (weeks and seasons). Raschke *et al.* (1973) reported on budget results from measurements obtained from an experiment on the Nimbus 3 satellite.

In this paper, the earth atmospheric radiation budgets are presented for a composite of 48 months over an intermittent period spanning 14 years (1964-1977) including 24 months of the more recent Nimbus 6 data obtained from the continuing earth radiation budget (ERB) experiment. The reported data is a result of a continuing compilation of radiation budget measurements which were first reported by Vonder Haar and Suomi (1971) (13 seasons of measurements) and later extended by Vonder Haar and Ellis[1] (29 months of selected radiation budget measurements).

This paper provides mean annual and seasonal radiation budgets determined with the composite satellite data set. The results are accurate to about $\pm 5\%$ (Vonder Haar and Ellis) and available for a resolution of about 10° latitude/longitude. A longer series of continued radiation budget measurements is desirable before meaningful interannual variations can be studied. The intermittent nature of the composite data set presented here prohibits such a study. However, a reasonable estimate of the variability of the radiation budget and its annual cycle is presented. The continued acquisition of data from the ERB experiment on Nimbus 6 (and Nimbus 7) will eventually supply a data set which will allow studies of the interannual variabilities of the radiation budget.

The determination of the radiative balance at the earth's surface is also essential to atmospheric modelling and, in particular, surface radiation budgets may provide some insight into the possible atmospheric and oceanic partitioning of the heat transport. An estimate of the surface budget is presented using a radiative transfer model. The radiative

---

[1] Vonder Haar, T. and J. Ellis, 1974: Atlas of radiation budget measurements from satellites. Atmospheric Science Paper No. 231, Colorado State University, Ft. Collins, CO, 180 pp.

transfer is an important part of the physics that must be incorporated in climate models and thus satellite based observations of the components of the radiation budget may serve as a test of model validity. In addition, comparisons between the current budget calculations and previous calculations are presented to highlight major differences arising from advances in our knowledge of radiative transfer in the atmosphere.

2. Satellite Data Sources

Data from satellite measurements of the reflected shortwave (planetary albedo), emitted longwave and net radiative fluxes have been compiled into global radiation budget climatologies.[2] The measurements from six different experiments comprise the composited data presented in this paper. Table 1 is a chronological summary of the satellite radiation budget data including the sample size in terms of months, seasons, and years. The measurements were of variable accuracy and resolution and the diameter of the half power region, indicative of the spatial resolution of the particular experiment, is included in the table. The 48 month set is a selective compilation of most of the satellite measurements at that time. Some of the available measurements were rejected because of discrepancies in the data set resulting primarily from instrumental problems (e.g. see Campbell and Vonder Haar[2] for details).

All satellites were for sun synchronous orbits sampling at just one local time during daylight hours (also included in Table 1). The data includes observations mainly for near noon orbits and possible diurnal biases in reflectance by varying solar elevation were corrected via a reflection model (e.g. Raschke et al., 1973). However, it must be recognized that this data processing cannot remove possible diurnal effects that arise from variations in the state of the atmosphere (such as cloud cover). In particular, the tropics which constitute roughly half of the surface area of the Earth and account for more than half of the radiative interaction with space, exhibit some fairly

---

[2] A more detailed discussion of the satellite data appears in the 1980 Colorado State University Report No. 320, "Climatology of Radiation Budget Measurements" by Campbell and Vonder Haar.

regular variations in temperature and cloudiness over the diurnal cycle (Riehl and Miller, 1978). Thus studies of the diurnal cycle employing geostationary satellite data are required to test the extent of the possible diurnal biases that may occur in the present data set.

Information concerning the satellite data and measurement uncertainties can be found in the report of Campbell and Vonder Haar[2]. The estimated absolute error of any individual month is about $\pm 5\%$ although the relative accuracy is higher. Specifically, the absolute values of net flux are accurate to about 10 $W \cdot m^{-2}$ but the relative variations of net flux (i.e. the gradients of net flux with respect to latitude and longitude) are significantly more accurate. The data before 1971 are essentially from Ellis and Vonder Haar[1] (1974) for medium resolution radiometers or wide angle, flat plate disc sensors. The 24 months of Nimbus 6 data (July 1975-June 1977) are obtained from wide angle and broad band sensors of the earth radiation budget experiment (ERB). Despite the instrumental differences between the basic data sets composited in this paper, it has been shown by Campbell and Vonder Haar that there is a consistency between the radiation budget components obtained from each set. The results presented below are for the annual radiation budget and the four seasonal budgets determined for the periods as indicated on Table 1.

The omnidirectional radiometers such as those described above measure the upwelling solar and IR radiation for all angles and, planetary albedo in particular, can be determined without the need to integrate over angle. This however is not true for scanning radiometers and integration is performed by employing rather dubious bidirectional reflection models. Unfortunately, the satellite sun

Table 1. Chronological list of earth orbiting satellites from which present radiation measurements were taken. The approximate local time at which each satellite crossed the equator during daylight hours appears in parenthesis. EX - experimental, N2 - Nimbus 2, N3 - Nimbus 3, N6 - Nimbus 6, E3 - Essa 3 and E7 - Essa 7.

Month	Season	1964	1965	1966	1968	1969	1970	1975	1976	1977	Sample Size
Jan	D.J.F.		Ex(10:30)			E7	N3		N6	N6	5
Feb			Ex(10:35)			E7			.	N6	4
Mar			Ex(10:40)			E7			.	N6	4
Apr	M.A.M.					N3(11:30)*			.	N6	3
May						N3			.	N6	3
Jun				N2(11:30)*		N3			.	N6	4
Jul	J.J.A.	Ex(8:30)				N3		N6(11:45)*	.		4
Aug		Ex(8:55)				N3		N6	.		4
Sep		Ex(9:15)						N6	.		3
Oct	S.O.N.	Ex(9:40)			E7(14:30)	N3		N6	.		5
Nov		Ex(10:05)			E7			N6	.		4
Dec	D.J.F.	Ex(10:30)		E3(14:40)	E7			N6	.		5
Annual		6	3	2	3	9	1	6	12	6	48

Resolution ≈ Half Power Diameter

Experimental	1280 km, 11.5°
ESSA3	
Nimbus 2	Averaged to 10° grid
ESSA7	2200 km, 20°
Nimbus 3	Averaged to 10° grid
Nimbus 6	1100 km, 10° (analyzed from 16°

*Albedo corrected for diurnal variation of reflection with directional reflectance model.

synchronous orbits do not pass directly over the polar regions and even the omnidirectional sensors view the earth's radiation from those regions at some oblique angle. Therefore, the determination of planetary albedo in the polar regions (poleward of 70^{o} latitude) are subject to some uncertainty as the validity of bidirection reflectance models remains uncertain.

3. Radiation Budget Measurements

The planetary net radiation budget is composed of incoming solar flux, reflected solar flux to space and the emitted terrestrial flux. At the top of the earth atmosphere boundary, the net radiation budget is defined as

$$N = (1-\alpha)S-I \qquad (1)$$

where α is the planetary albedo, S is the incoming solar flux based on the solar constant of 1376 $W.m^2$ (Hickey et al., 1980) and corrected for variations in sun-earth distance, day length and solar declination and I is the emitted flux (IR) by the earth atmosphere system. The following analysis presents composited measurements of the quantities N, α and I. The net flux distribution N provides the necessary forcing of the atmospheric circulation and the gradient of this quantity (with latitide and longitude) is a reasonable indication of the extent of this forcing (Vonder Haar and Suomi, 1971).

a. Zonal radiation budgets

The latitudinal distribution of the annual and seasonal net radiative energy input into the earth atmospheric system, the planetary albedo and the outgoing (emitted) longwave radiation are shown in Fig. 1a, b, c, d and e for the 48 month composite data set. In the annual profiles, approximate symmetry in N, α and I prevails between the northern and southern hemispheres. The minimum in emitted flux near the equator ($5^{o}N$) is a result of the cloudiness associated with the ITCZ. It is apparent from the seasonal profiles how this minimum migrates about the equator. The high emission around $25^{o}S$ and $25^{o}N$ are indicative of warm desert like regions (both over land and over ocean). The annual

Fig. 1a

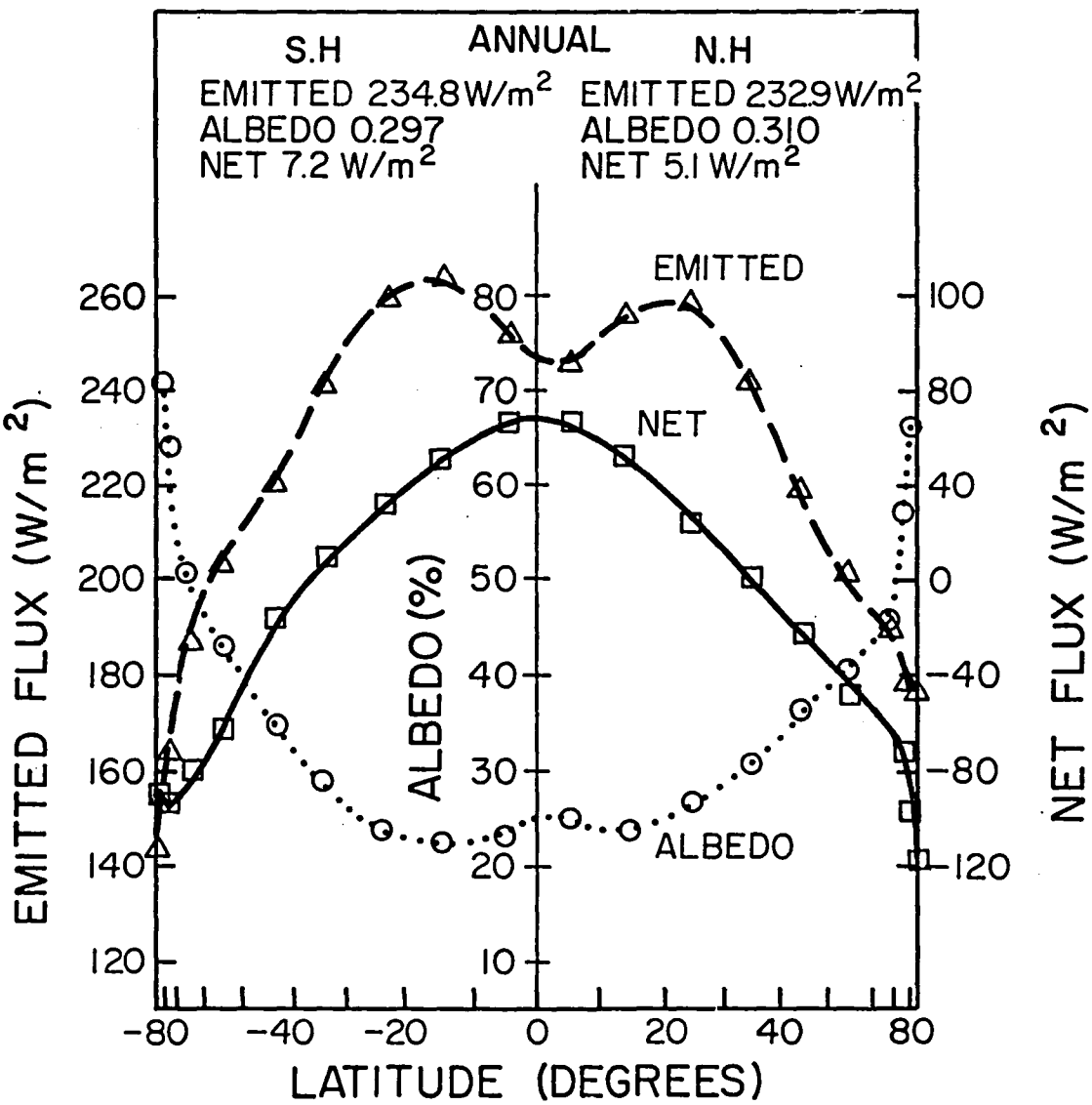
S.H
ANNUAL
N.H
EMITTED 234.8W/m2
ALBEDO 0.297
NET 7.2 W/m2
EMITTED 232.9W/m2
ALBEDO 0.310
NET 5.1 W/m2
EMITTED
NET
ALBEDO
EMITTED FLUX (W/m 2)
ALBEDO (%)
NET FLUX (W/m 2)
260
240
220
200
180
160
140
120
80
70
60
50
40
30
20
10
100
80
40
0
-40
-80
-120
-80
-40
-20
0
20
40
80
LATITUDE (DEGREES)

Fig. 1b

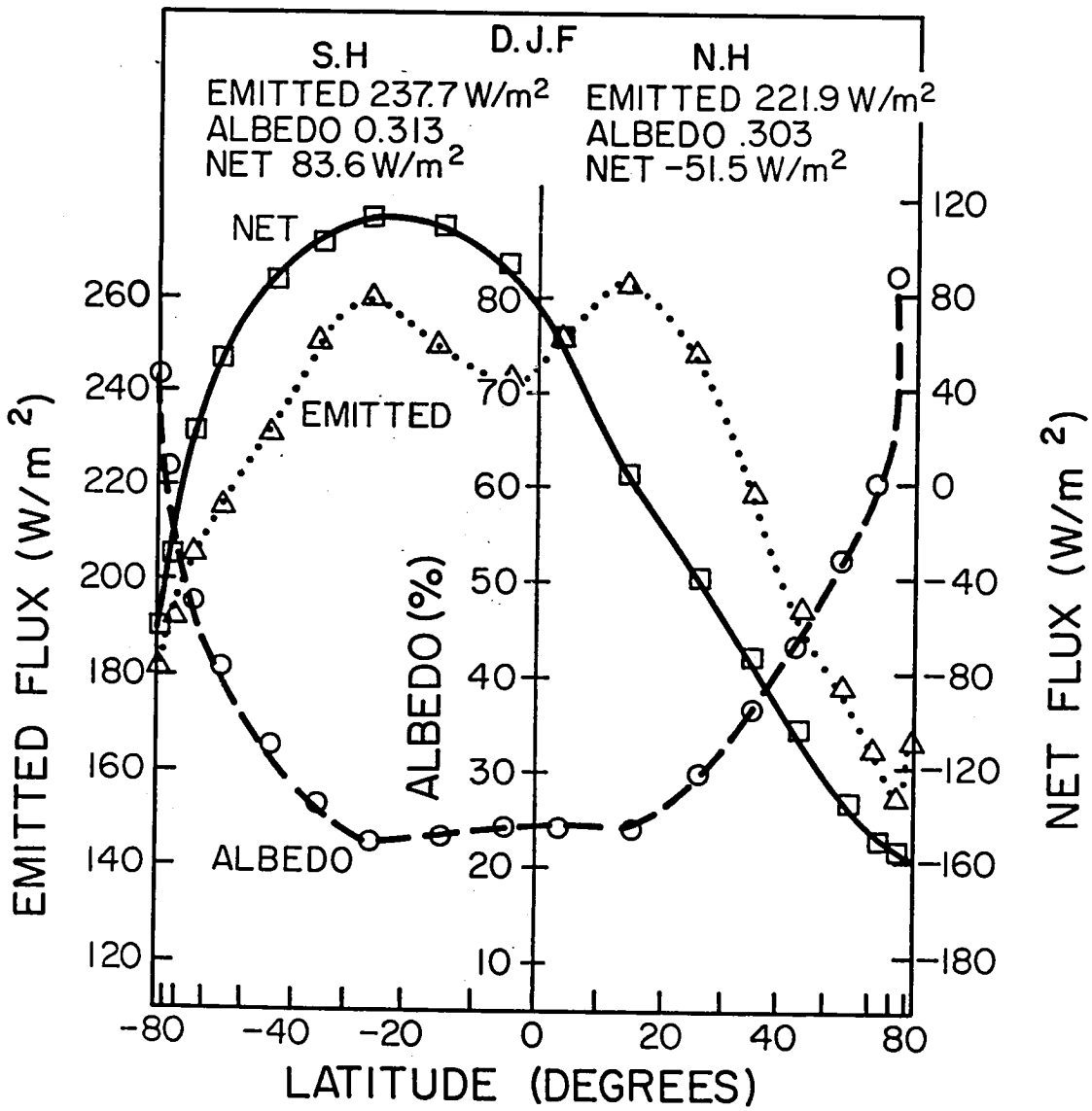
S.H
D.J.F
N.H
EMITTED 237.7 W/m²
ALBEDO 0.313
NET 83.6 W/m²
EMITTED 221.9 W/m²
ALBEDO .303
NET -51.5 W/m²
NET
EMITTED
ALBEDO
EMITTED FLUX (W/m²)
ALBEDO (%)
NET FLUX (W/m²)
LATITUDE (DEGREES)
260
240
220
200
180
160
140
120
80
70
60
50
40
30
20
10
120
80
40
0
-40
-80
-120
-160
-180
-80
-40
-20
0
20
40
80

Fig. 1c

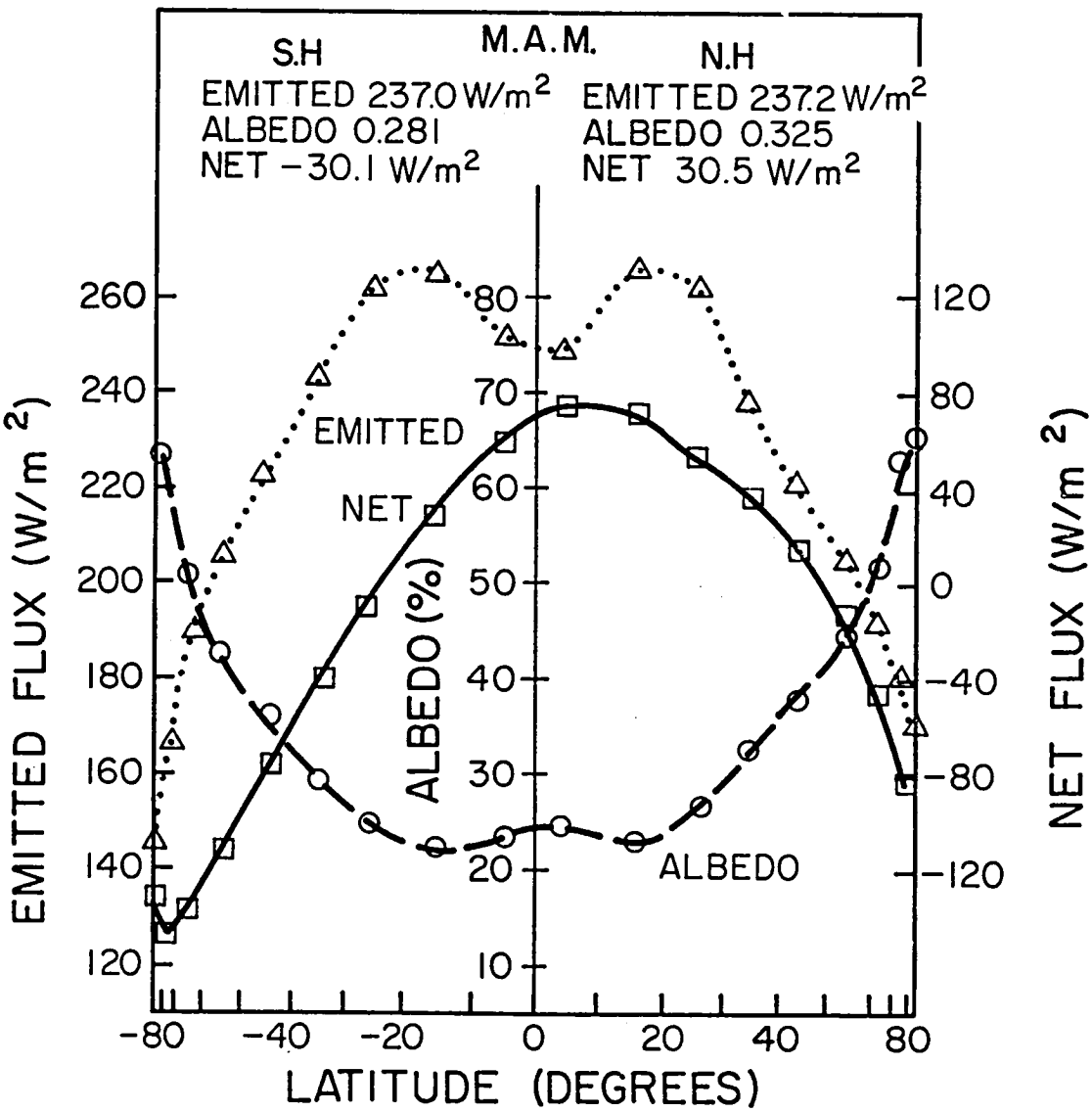
S.H
M.A.M.
N.H
EMITTED 237.0 W/m²
ALBEDO 0.281
NET −30.1 W/m²
EMITTED 237.2 W/m²
ALBEDO 0.325
NET 30.5 W/m²
EMITTED
NET
ALBEDO
EMITTED FLUX (W/m²)
ALBEDO (%)
NET FLUX (W/m²)
LATITUDE (DEGREES)
260
240
220
200
180
160
140
120
80
70
60
50
40
30
20
10
120
80
40
0
−40
−80
−120
−80
−40
−20
0
20
40
80

Fig. 1d

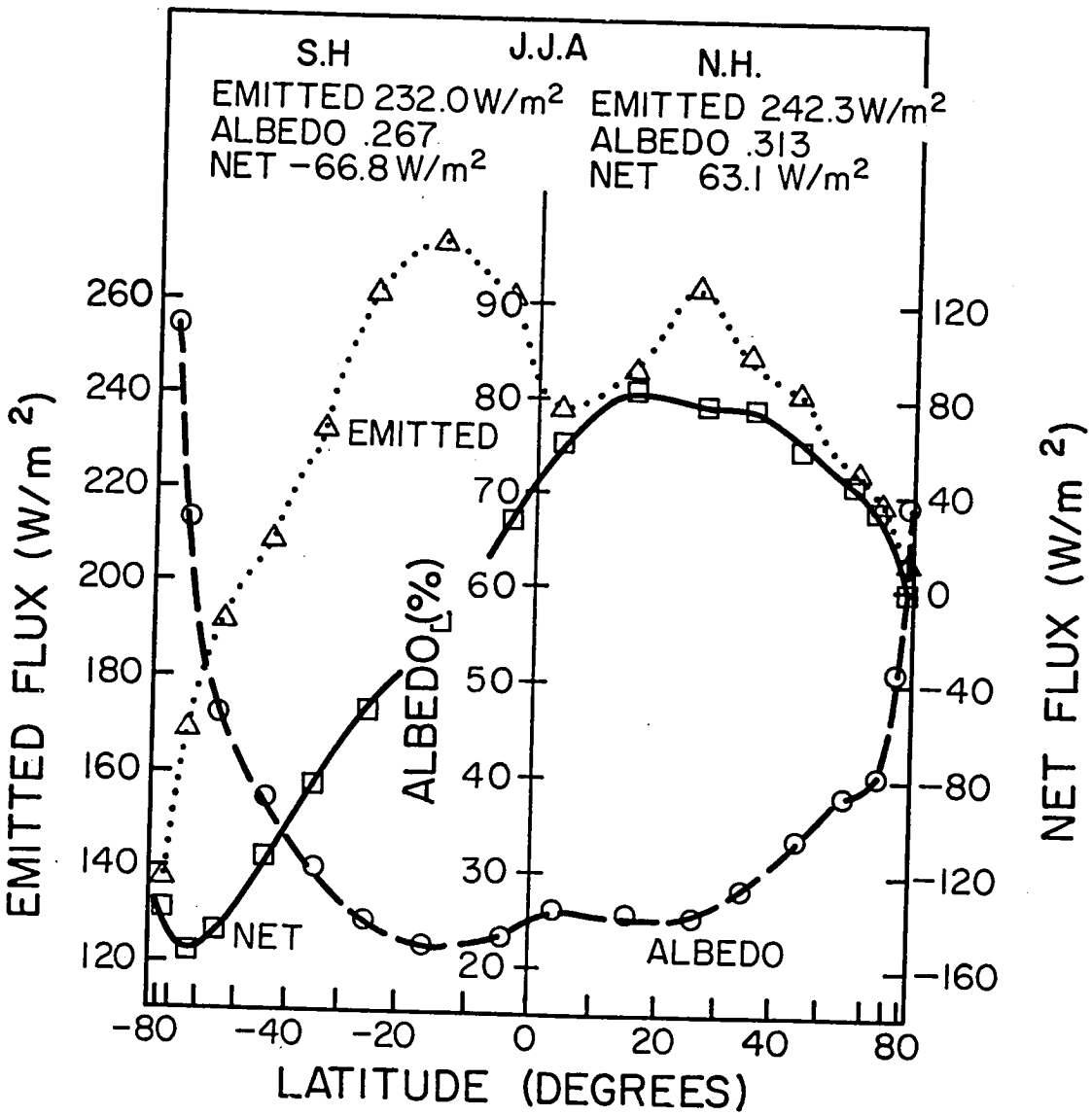
S.H
J.J.A
N.H.
EMITTED 232.0W/m²
ALBEDO .267
NET −66.8 W/m²
EMITTED 242.3W/m²
ALBEDO .313
NET 63.1 W/m²
EMITTED
NET
ALBEDO
EMITTED FLUX (W/m²)
ALBEDO (%)
NET FLUX (W/m²)
LATITUDE (DEGREES)
260
240
220
200
180
160
140
120
90
80
70
60
50
40
30
20
120
80
40
0
−40
−80
−120
−160
−80
−40
−20
0
20
40
80

Fig. 1e

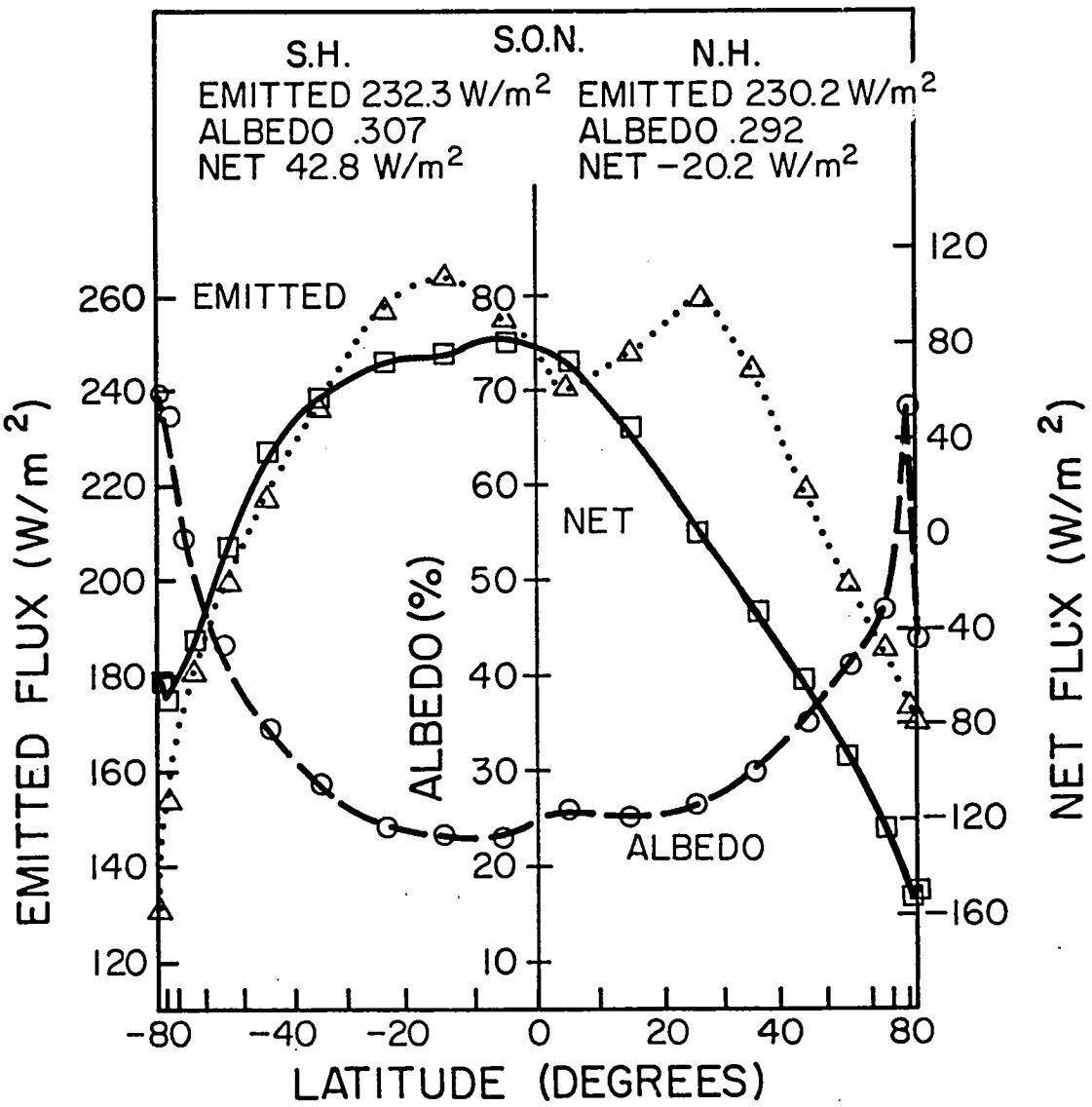
S.H.
S.O.N.
N.H.
EMITTED 232.3 W/m2
ALBEDO .307
NET 42.8 W/m2
EMITTED 230.2 W/m2
ALBEDO .292
NET −20.2 W/m2
EMITTED
NET
ALBEDO
EMITTED FLUX (W/m 2)
ALBEDO (%)
NET FLUX (W/m 2)
LATITUDE (DEGREES)
260
240
220
200
180
160
140
120
80
70
60
50
40
30
20
10
120
80
40
0
−40
−80
−120
−160
−80
−40
−20
0
20
40
80

profile of planetary albedo, on the other hand, displays a maximum at $5^{o}N$ in concert with the minimum in the emitted flux. The variation of albedo poleward of the subtropics is similar for each season and is caused largely by the change in mean sun angle with latitude. In the tropical region, the planetary albedo variation is influenced more by weather disturbances and their attendant cloud distributions.

The qualitative features of the seasonal net flux profiles displayed in Fig. 1 show a maximum net radiative input in the tropics which migrates according to the sun's position and a net deficit of radiative energy in the polar regions. Also shown in Fig. 1 are the hemispheric and global averages of the emitted flux, albedo and net flux. The annual global average emitted flux is 234 ± 2 $W.m^{2}$, planetary albedo is 0.30 $\pm$ 0.01 and net flux is 6 $W.m^{-2}$. The small positive net flux value for the annual, global average is indicative of the absolute magnitude of error associated with the net flux determinations. While the absolute error is of the order of 10 $W.m^{-2}$, the relative error and thus gradients of net flux are much smaller (Campbell and Vonder Haar, 1980). The slight differences in the radiation budget quantities between the Northern and Southern hemispheres may be attributed, in part, to the differences in land ocean extent between the hemispheres.

b. Annual variations

There is a significant amount of month to month variation in the radiation budget quantities. This is exemplified in Fig. 2 which shows the annual variation of the mean values of emitted flux, planetary albedo and net flux. These values are area means from $70^{o}N$ to $70^{o}S$. Global integrations were not performed in this case as some data were

missing poleward of 70°N and S for individual months. The annual cycle in the globally integrated net flux, previously reported by Ellis et al., (1978), has an amplitude of about 13 $W.m^{-2}$. The credibility of such a cycle can be qualitatively assessed from the heat budget studies of Ellis et al. who showed that the change of heat content (storage) of the Earth possessed similar amplitudes and phases to the planetary net flux. Their global heat storage estimates were computed by independent in situ measurements of temperature.

The annual cycle of globally integrated net flux is due, in part, to the annual variation of the globally averaged integrated solar flux input into the top of the Earth atmosphere system. This variation, shown in Fig. 2 as a dashed curve, has an amplitude of 11 $W.m^{-2}$ and is purely externally forced dependent only on the earth sun geometry. In fact, it is shown below that the variability of the global distribution of net flux input at the top of the atmosphere is primarily determined by this external forcing. The residual of the cycle is likely to be a result of the hemispheric differences in land-ocean extent. For example, the annual cycle of planetary albedo is likely to be determined by the hemispheric differences of snow ice extent which provides large albedos (particularly in the polar regions). Further, the annual variation in the longwave emission to space occurs because of unequal temperature responses between the land and water surfaces and the asymetrical distribution of these between the Northern and Southern hemisphere.

Fig. 3 presents the interannual variations of the hemispherically averaged net flux which are presented for the seasonal intervals specified above. The annual, global cycle in the net flux (dashed curve)

Fig. 2

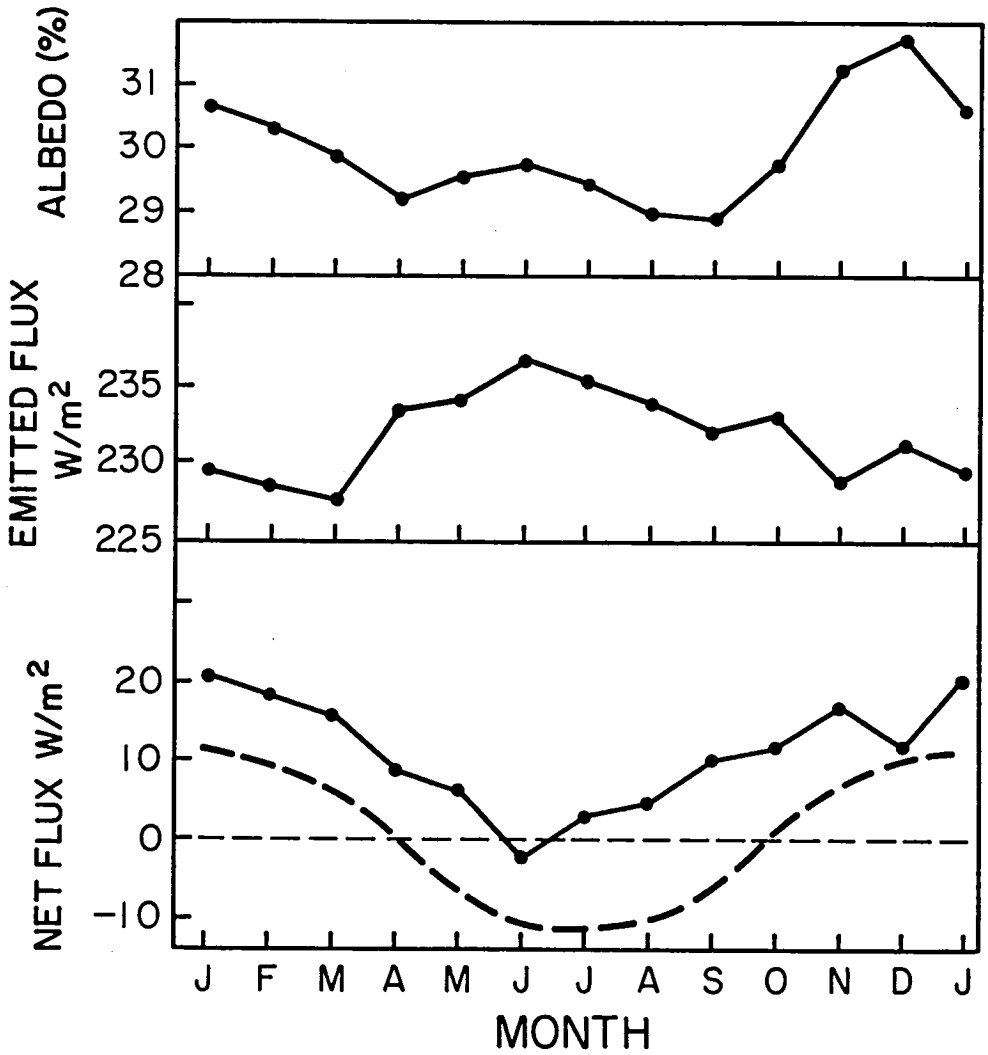
ALBEDO (%)
31
30
29
28
EMITTED FLUX W/m²
235
230
225
NET FLUX W/m²
20
10
0
-10
J F M A M J J A S O N D J
MONTH

Fig. 3

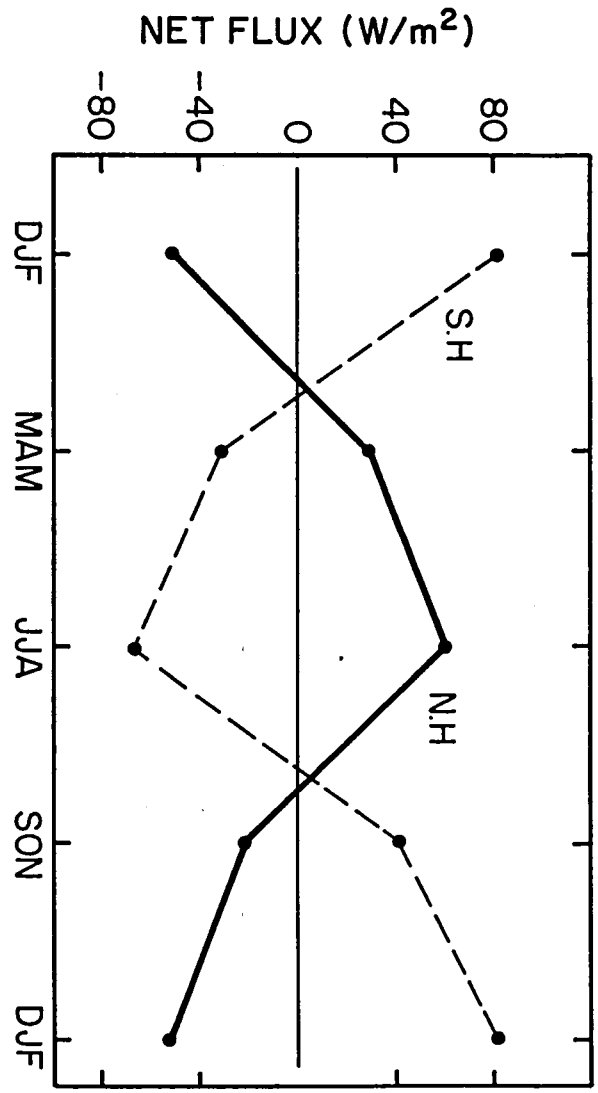

is in phase with the cycle of the southern hemisphere net flux, partly due to the external controls associated with the earth-sun geometry and partly as a result of land sea differences and the related radiative responses between the hemisphere. For both hemispheres, the largest changes in the net flux from one season to another occur for the transition from solstice to equinox. This marked variation is also evident in the global maps of net flux discussed below.

c. Global Distributions

Figs. 4 through 8, respectively, show the global distributions of emitted flux, planetary albedo and net flux averaged for the mean annual and designated seasonal periods. The annual albedo maps reveal a distinct ocean continent contrast equatorward of 30^{o}N and S and the high reaching convective clouds associated with the Asian monsoon are particularly apparent especially when related to the low emission (less than 230 $W.m^{-2}$) evident in Fig. 4a for that region. Generally, a net radiation gain prevails over ocean regions which may be directly attributed to the lower albedo over oceans compared to the zonal average. Poleward of 30^{o}N and S, the albedo is zonally uniform except for some slight continental influence (e.g. over North America) in the Northern hemisphere. This zonally uniform structure is evidence of the dominant dependence of the planetary albedo on the sun's position.

A distinct feature of the net flux distribution is the relatively high input of net radiative energy in the Southeast Asian region. There is some evidence for suggesting the presence of low persistent stratus decks along the west coastal areas of North and South America, and Africa in the maps of emitted radiation (e.g. distinct maxima west of Africa and South America) and albedo. The net flux maps accordingly show

Fig. 4

ANNUAL EMITTED

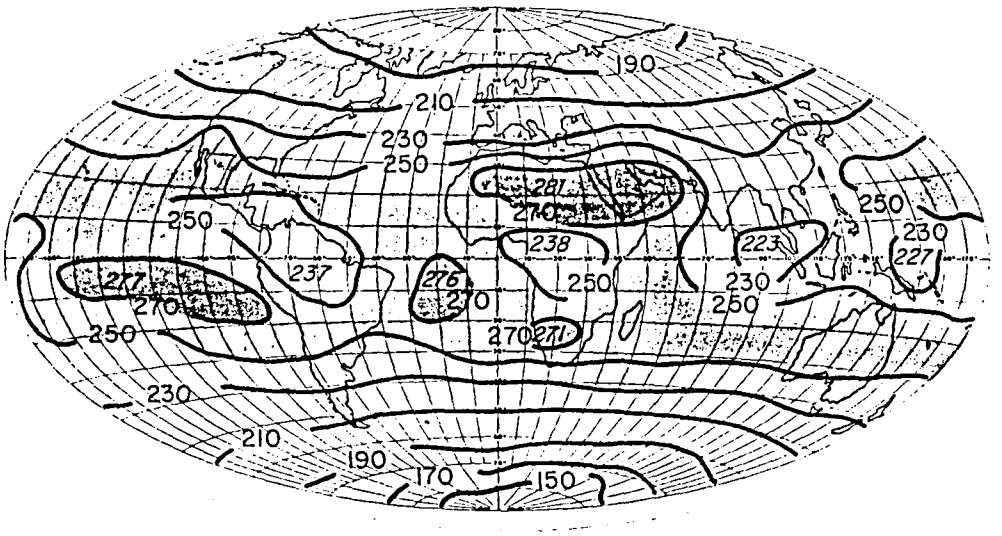

ANNUAL ALBEDO

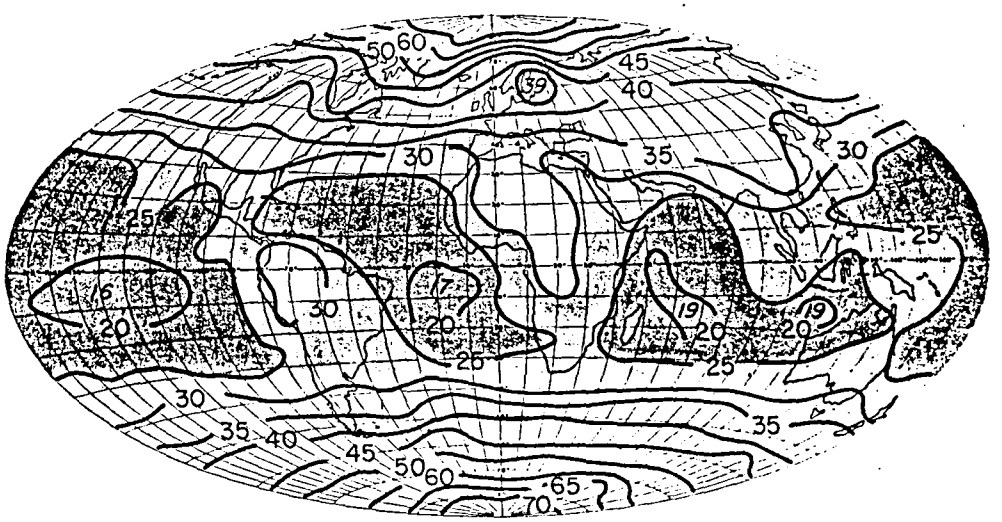

ANNUAL NET

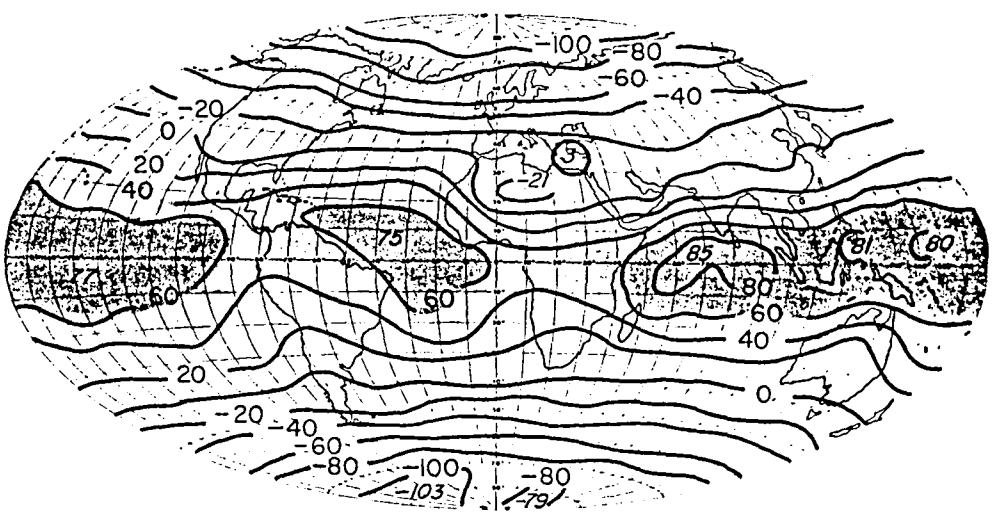

Fig. 5

D.J.F EMITTED

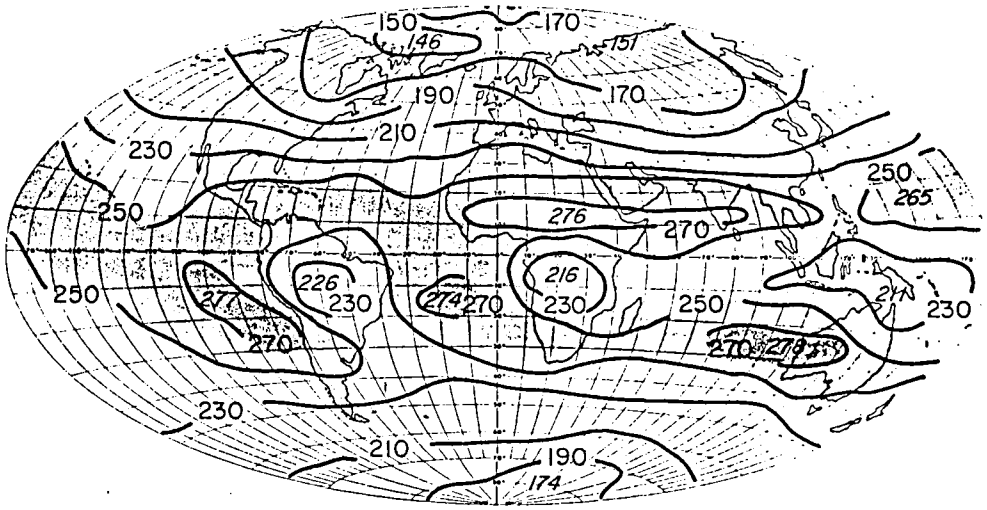

D.J.F ALBEDO

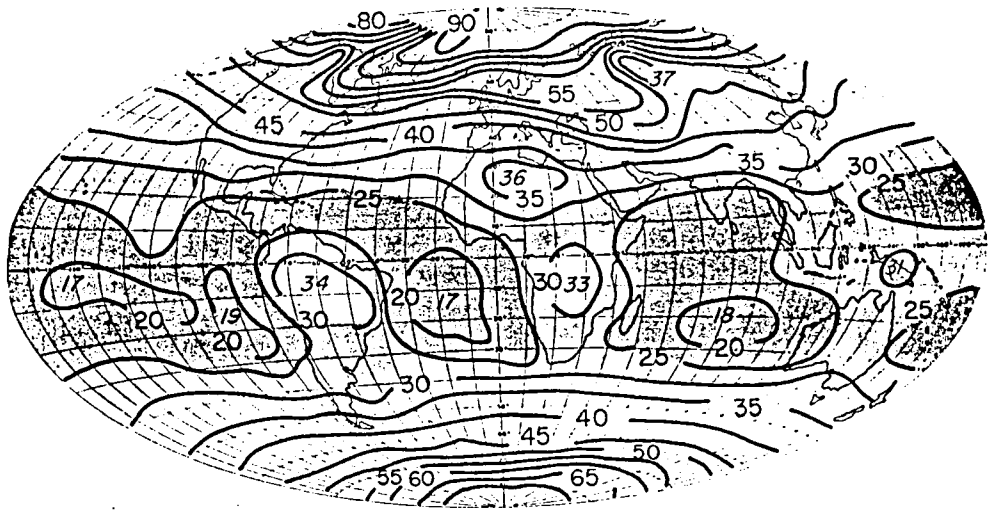

D.J.F NET

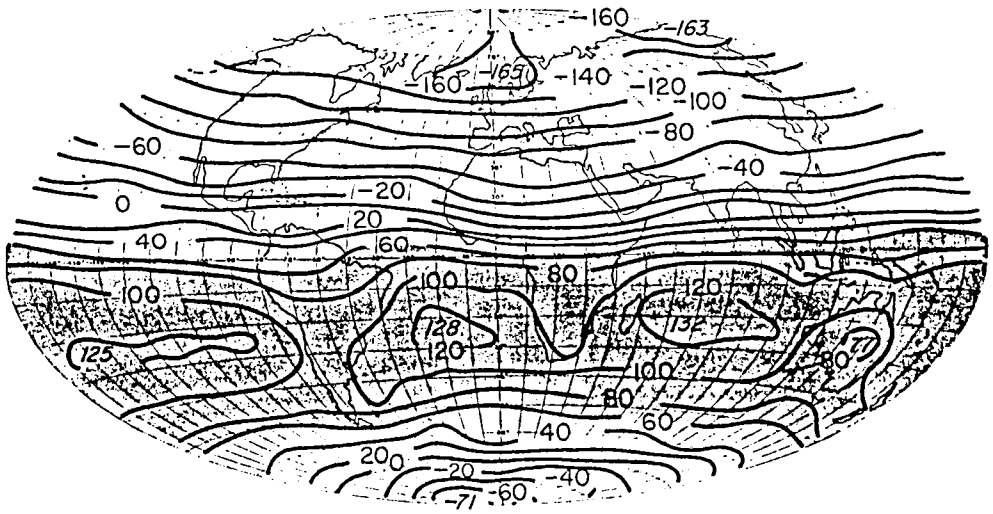

Fig. 6

M.A.M EMITTED

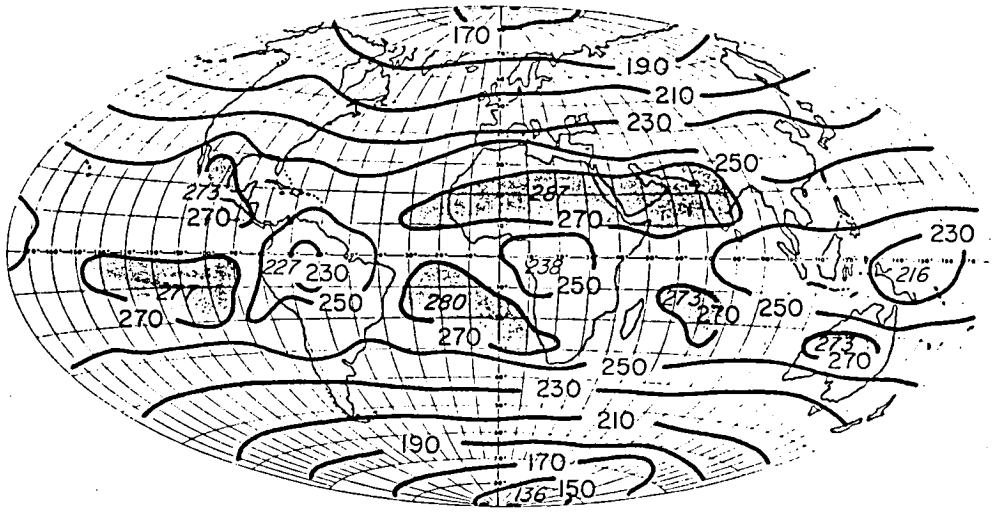

M.A.M ALBEDO

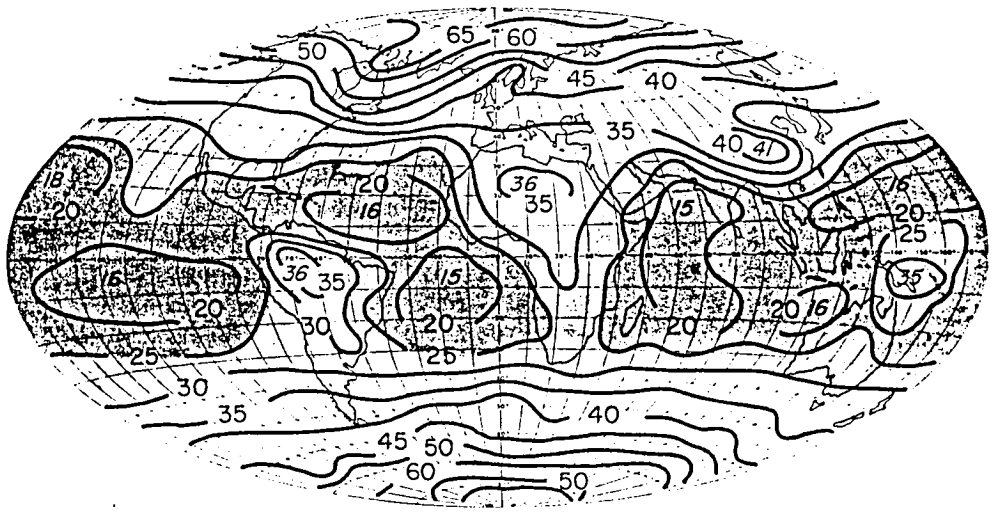

M.A.M NET

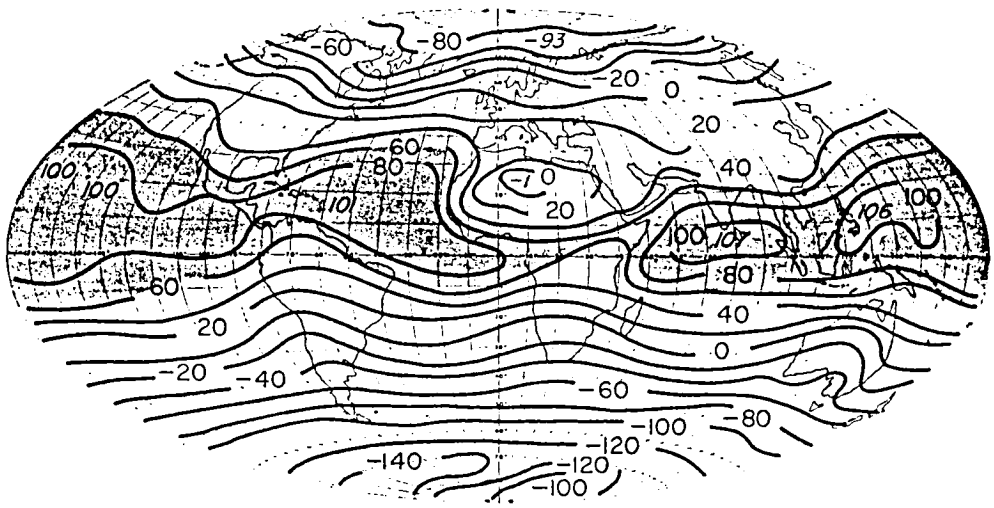

Fig. 7

J.J.A. EMITTED

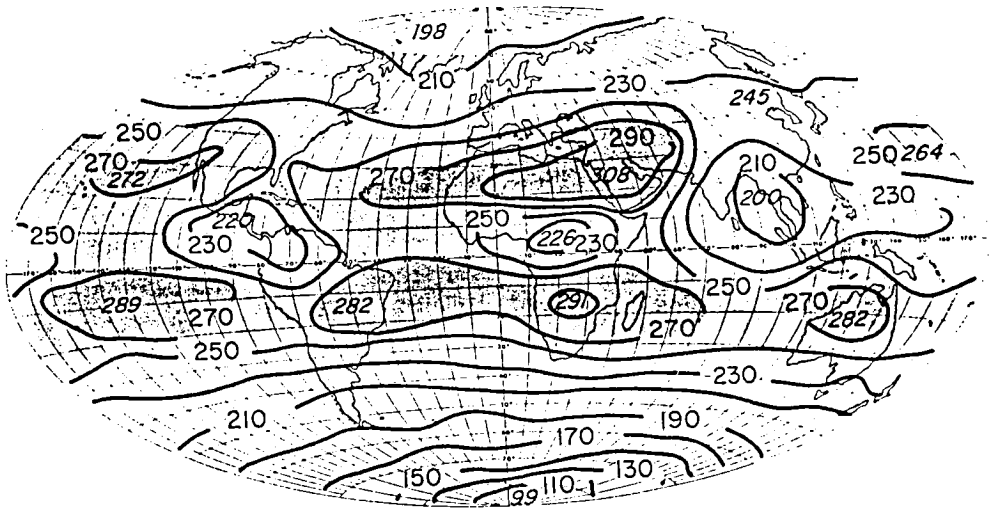

J.J.A ALBEDO

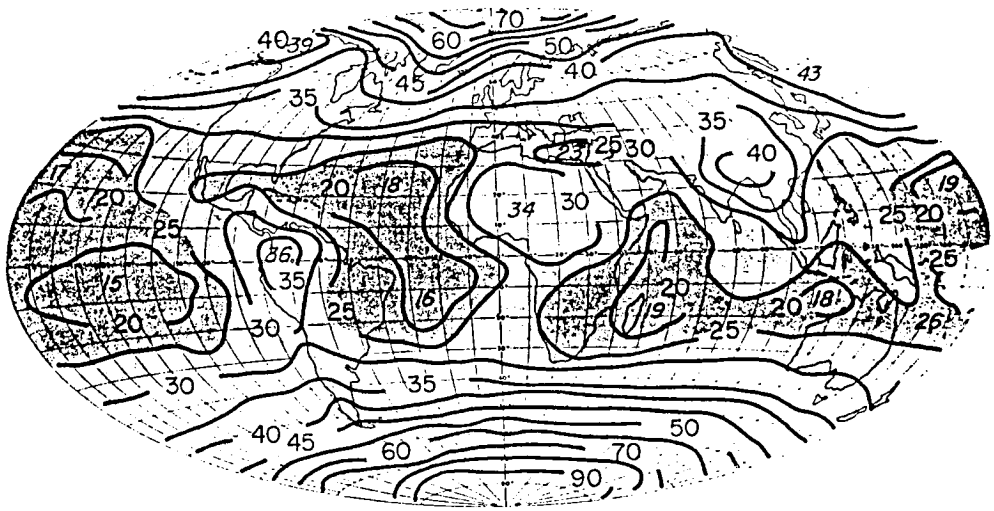

J.J.A. NET

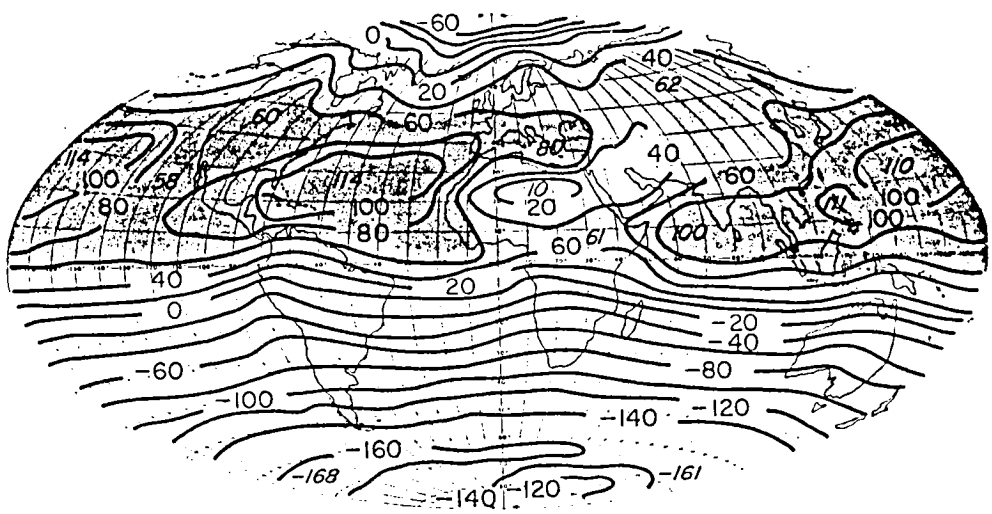

Fig. 8

S.O.N. EMITTED

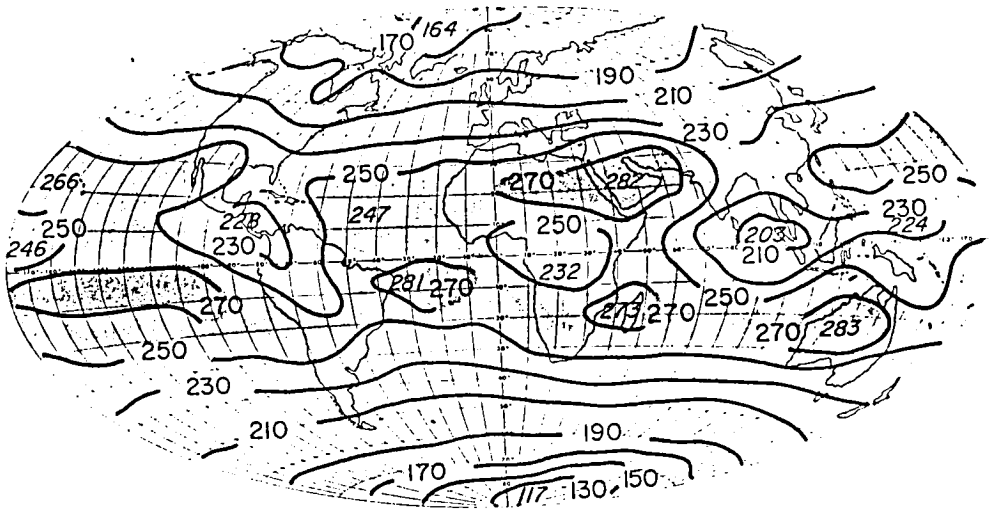

S.O.N. ALBEDO

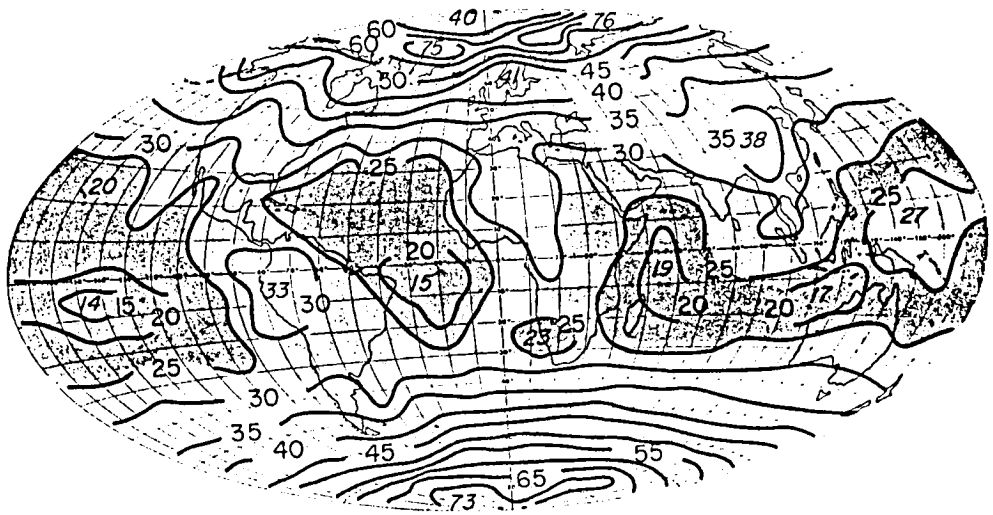

S.O.N NET

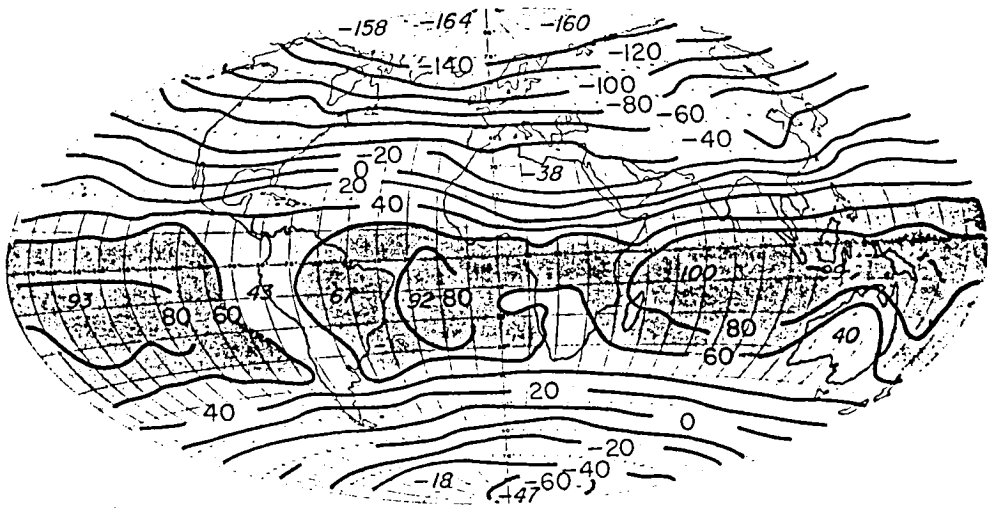

distinct regions of relative low energy input particularly west of South America and South Africa and a minimum over the desert regions. It is interesting to consider that the oceanic deserts (regions of low persistent stratus over the oceans, e.g. Vonder Haar, 1972) and the continental deserts (e.g. African, Arabian, and to a lesser extent the Australian desert regions) appear as regions of relative low net radiation. Charney (1975) employed a simple conceptual model to demonstrate that the net radiative heat loss over the Saharan Desert as evident in Fig. 4c, produces a positive feedback mechanism to amplify the descending branch of the mean Hadley circulation. It is interesting to speculate on similar effects in the oceanic desert regions which are more variable depending on cloud distribution.

The maps presented in Fig. 4 are for the mean annual case, and thus all daily and even seasonal anomalies are smoothed. Even so, at lower latitudes in particular, regions of relative gain and loss of energy are evident within a given zone. For example, distinct variations are evident in the net fluxes in the tropical zones where the deserts of Africa and Arabia appear as negative or small positive anomalies and the convective regions near Asia are large positive anomalies in net flux. Thus numerical simulations of the atmospheric or oceanic circulation cannot include forcing functions only as a function of latitude (i.e. of solar declination). Stephens and Webster (1979), for example, indicated that zonal variations in the radiative forcing cannot be simulated without zonal variations in cloud cover.

The seasonal maps of net flux show that regions of high net radiative input are distinctly non-uniform in structure with the excursion of this region north or south governed by the position of the sun.

Poleward of this band of high energy input is a fairly uniform, zonal net flux distribution, more so than for the individual components of emitted flux and albedo. Further, and in concert with the changes of hemispheric net flux discussed in relation to Fig 3, the most dramatic changes of net flux distribution occur for the transition from solstice to equinox.

The albedos are generally negatively correlated with the emitted flux except over the desert regions discussed above. This reciprocity between emitted flux and cloud is a direct result of the effect of cloud on these components. Simply, the increased loss of energy to space by reflection from the cloud is offset by the decreased emission from the (colder) cloud tops. This reciprocity is evident in each of the seasonal maps producing net flux distributions which are more zonal in structure than either the maps of the two components α or I.

Other distinct features of the seasonal maps are the similarities of planetary albedo in the tropical regions for which a distinct ocean continent contrast is evident for all seasons. Secondly, there are three regions of significantly low emission (particularly for JJA) which contrast adjoining zones. These are located west of Panama, over the South African continent and in the Southeast Asian region. These regions persist for all seasons but display a distinct southward excursion for the D.J.F. map. The net flux over the Southeat Asian region displays a distinct net flux positive anomaly for most seasons but especially for MAM and JJA. It is interesting that, for this case, the cancellation effect discussed above does not occur and perhaps suggests a dominance of high cloud in this region. Finally, the relative low net radiative input west of the major continents of the Southern hemisphere is most pronounced

for SON. This feature, as discussed above, persists in the annual maps of net flux.

d. Variance in the annual cycle

As evident in Fig. 3, the global net flux, planetary albedo and emitted flux display a distinct annual cycle. However, this annual cycle is more pronounced for a given region. For example, Fig. 9 shows the annual cycle in net flux, emitted flux and albedo for the Southeast Asian region located at 70°-80°E, 10°-30°N. A study of the albedo cycle clearly indicates the distinct maximum associated with the height of the monsoon activity as measured by intensification of cloud amount. The emitted flux, by contrast, displays a pronounced minimum in concert with the albedo maximum. The combined effect is that the total energy reradiated to space is quite uniform despite the probable large change in cloudiness and the annual cycle of net flux is similar to the cycle of solar radiation input (a function only of earth-sun geometry). The profiles shown in Fig. 9 are a dramatic example of the reciprocity between the increased outgoing shortwave flux by reflection and the decreased emission to space from the colder cloud tops. However, it is very important to note that the regions and conditions that evidence a lack of reciprocity are considerable. These should be the focus of radiation budget modeling studies, for here the impact on climate is potentially the greatest.

The mean monthly values of net flux for each of the grid areas were employed to determine the maps of the amplitudes of both the annual and semiannual cycles (Fig. 10a and b). Also shown in Figs. 11a and b is the percentage of the total variance explained by the cycles, the total variance being defined as the variance in the 12 monthly maps. The amplitudes of

Fig. 9

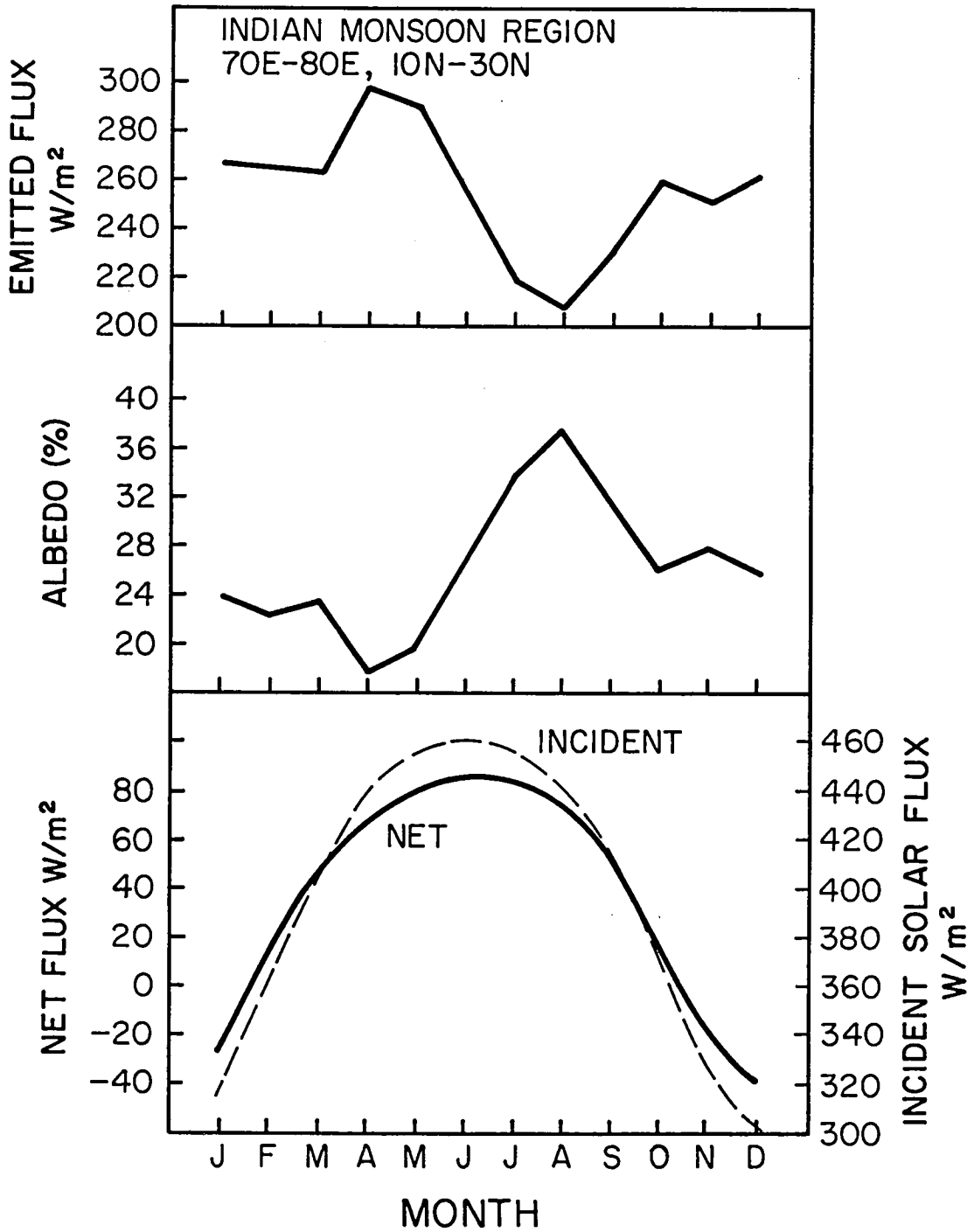
INDIAN MONSOON REGION
70E-80E, 10N-30N
EMITTED FLUX W/m²
300
280
260
240
220
200
ALBEDO (%)
40
36
32
28
24
20
NET FLUX W/m²
80
60
40
20
0
-20
-40
INCIDENT
NET
460
440
420
400
380
360
340
320
300
INCIDENT SOLAR FLUX W/m²
J F M A M J J A S O N D
MONTH

N-AMPLITUDE (W/m^2)

ANNUAL

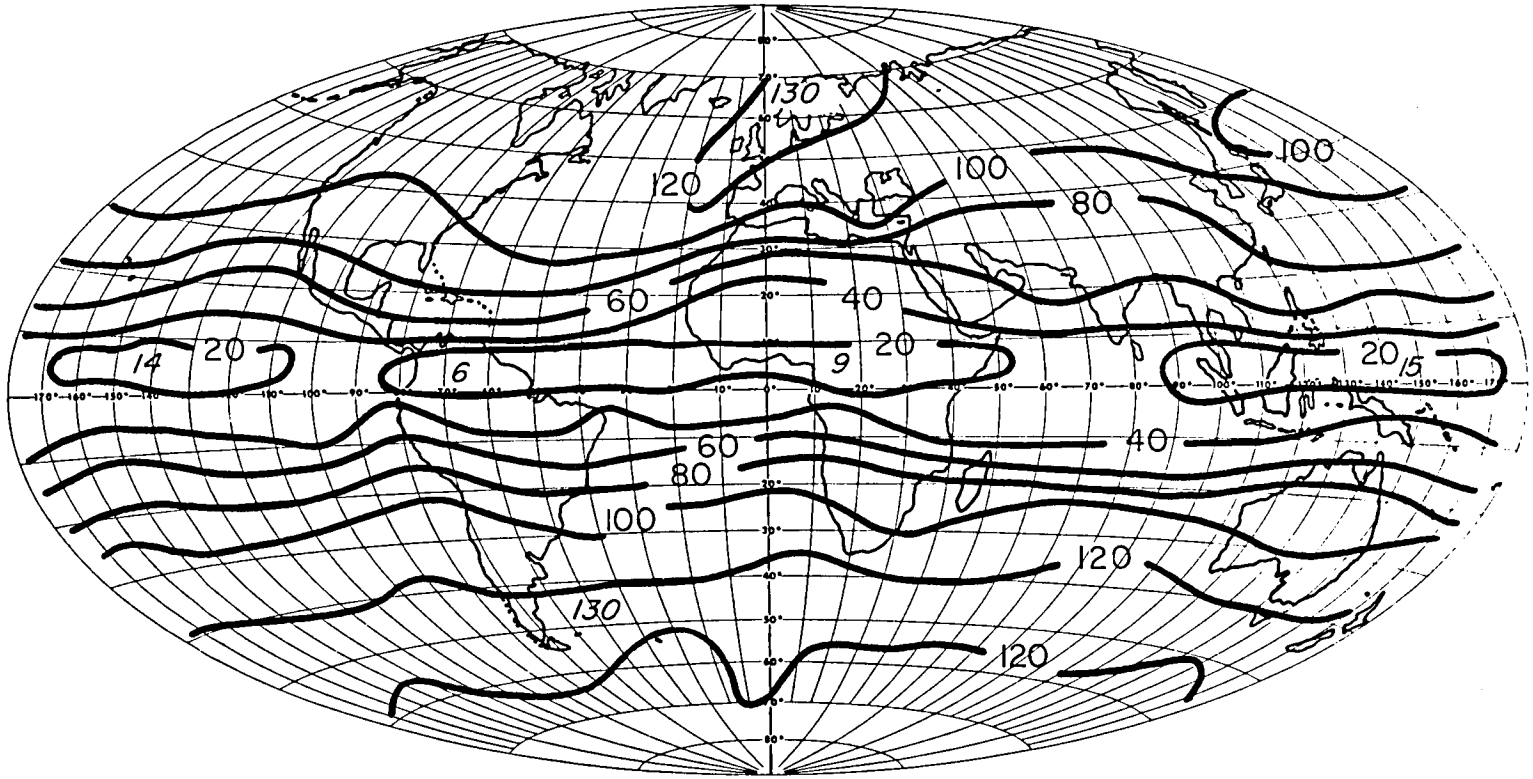

Fig. 10a

N−AMPLITUDE (W/m^2)
SEMI-ANNUAL

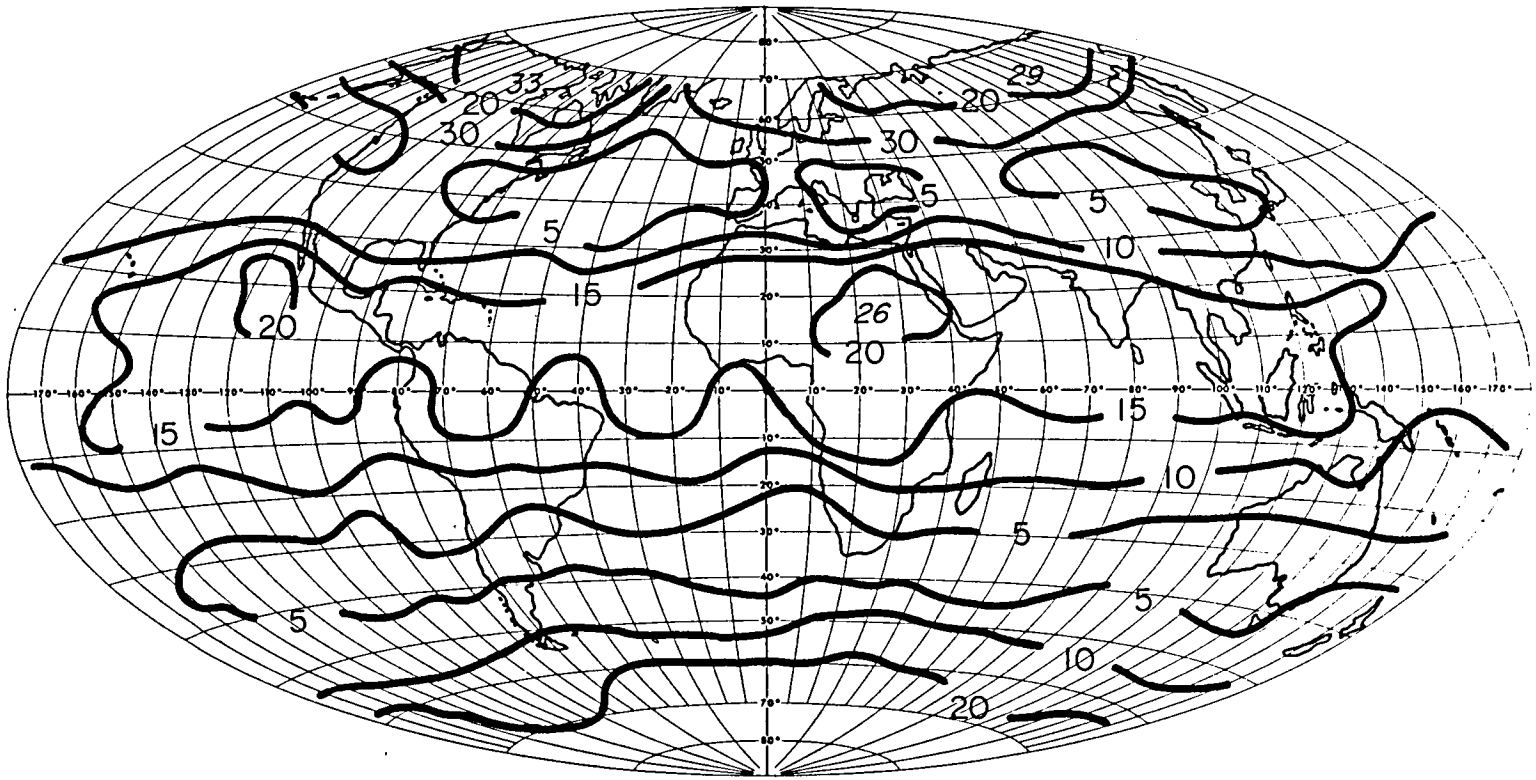

Fig. 10b

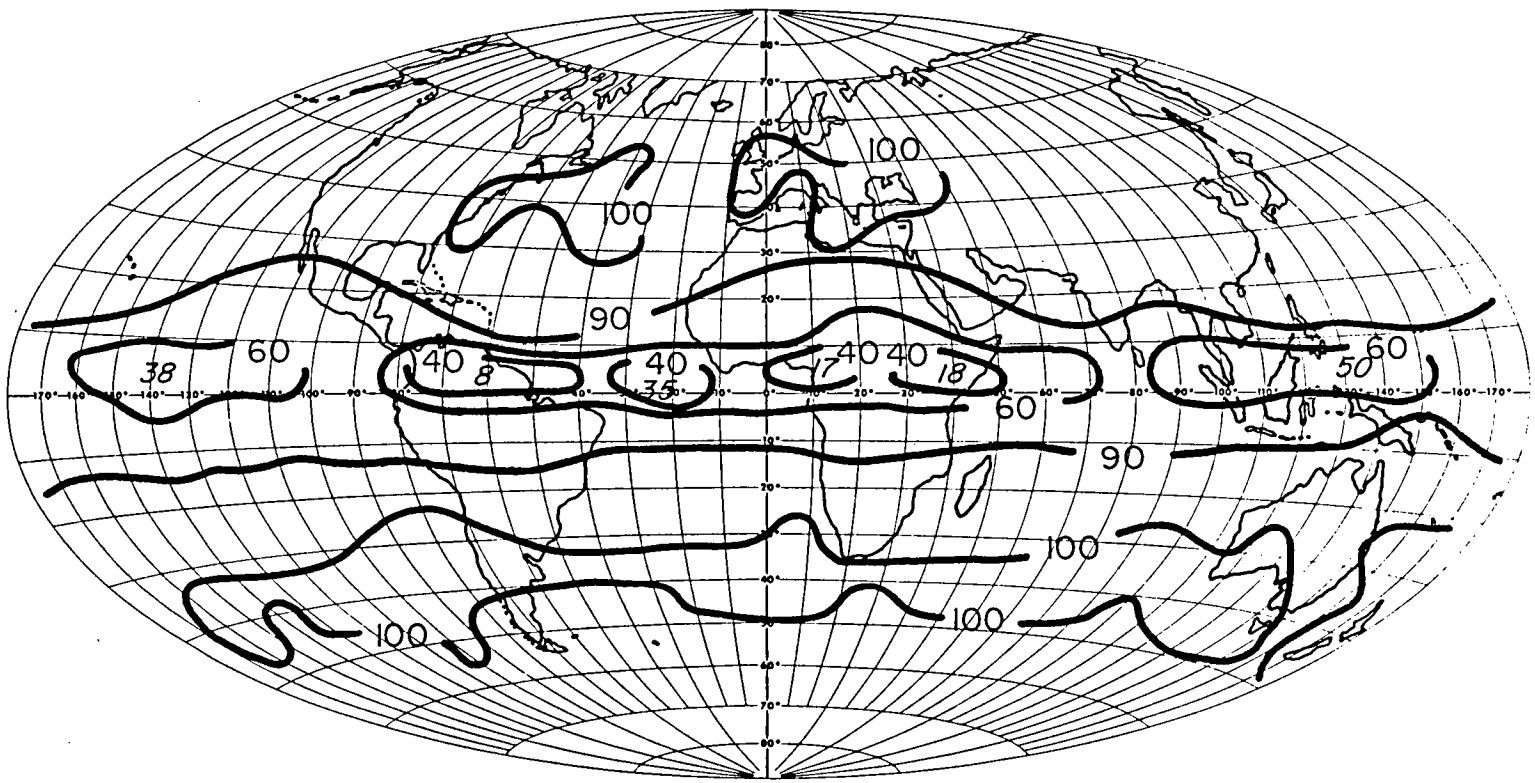
N-EXPLAINED VARIANCE (%)
ANNUAL
100
100
90
60
38
40
8
40
35
17
40
40
18
60
50
60
90
100
100

Fig. 11a

N-EXPLAINED VARIANCE (%)
SEMI-ANNUAL

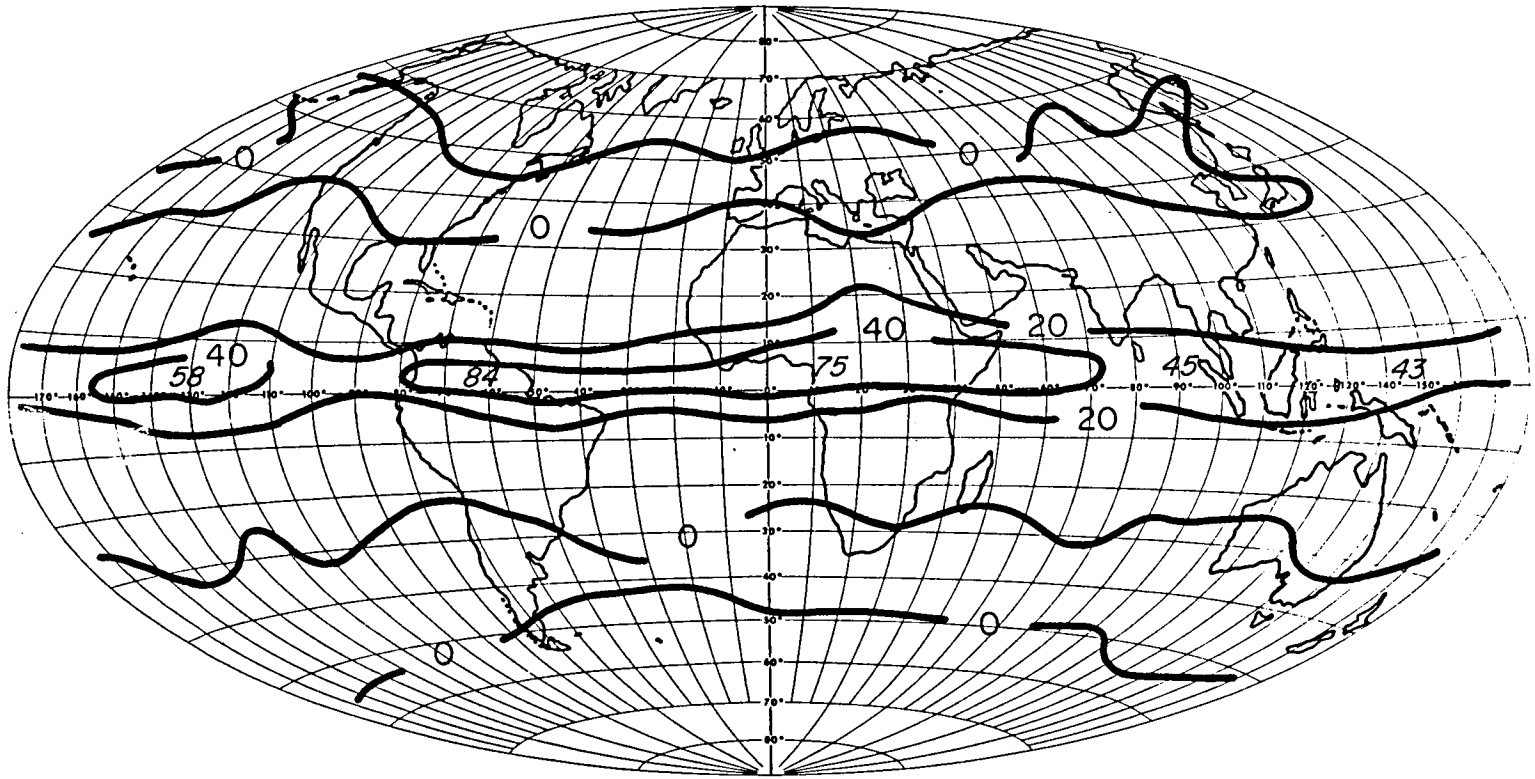

Fig. 11b

the annual cycle are largest in the higher latitudes which can be attributed to the more dramatic change of solar elevation during the year. The amplitudes are smaller in the tropics with a well-defined narrow belt of minimum values centered at the equator. The amplitudes of the semiannual cycle, on the other hand, displays a maximum equatorward of about 20^{o} latitude (in part from the "passage" of the sun) and also a distinct maximum in the polar regions.

The total variance in the net flux, shown in Figs. 11a and b, is almost completely explained (within a few percent or about 6 $W.m^{-2}$) by the annual cycle poleward of about 20^{o} latitude and the combined annual plus semiannual cycle equatorward of 20^{o}. It is therefore evident that the variation in net flux at the top of the earth atmosphere system arises almost exclusively from the variations of the external forcings resulting from the regular change in solar declination throughout the year which imposes the two basic cycles. Thus the variation of net flux arises from the changing input energy to the system and the exitant energy composed of the emitted and reflected radiant fluxes remains roughly uniform with a mutual cancellation occurring between the two.

Fig. 12a presents the amplitude of the annual cycle of emitted flux. A distinct ocean continent contrast is evident (particularly in the Northern Hemisphere) with generally smaller amplitudes over the ocean regions. This suggests that the oceans perhaps provide a stabilization of outgoing longwave radiation. There are three specific regions of large amplitudes, one centered over the Bay of Bengal, one west of Panama and one centered near the Middle East. The Australasian monsoon region also displays a larger amplitude in the annual cycle than for the adjacent regions. The large amplitudes over the monsoon regions are influenced by the cloud distributions associated with the monsoon.

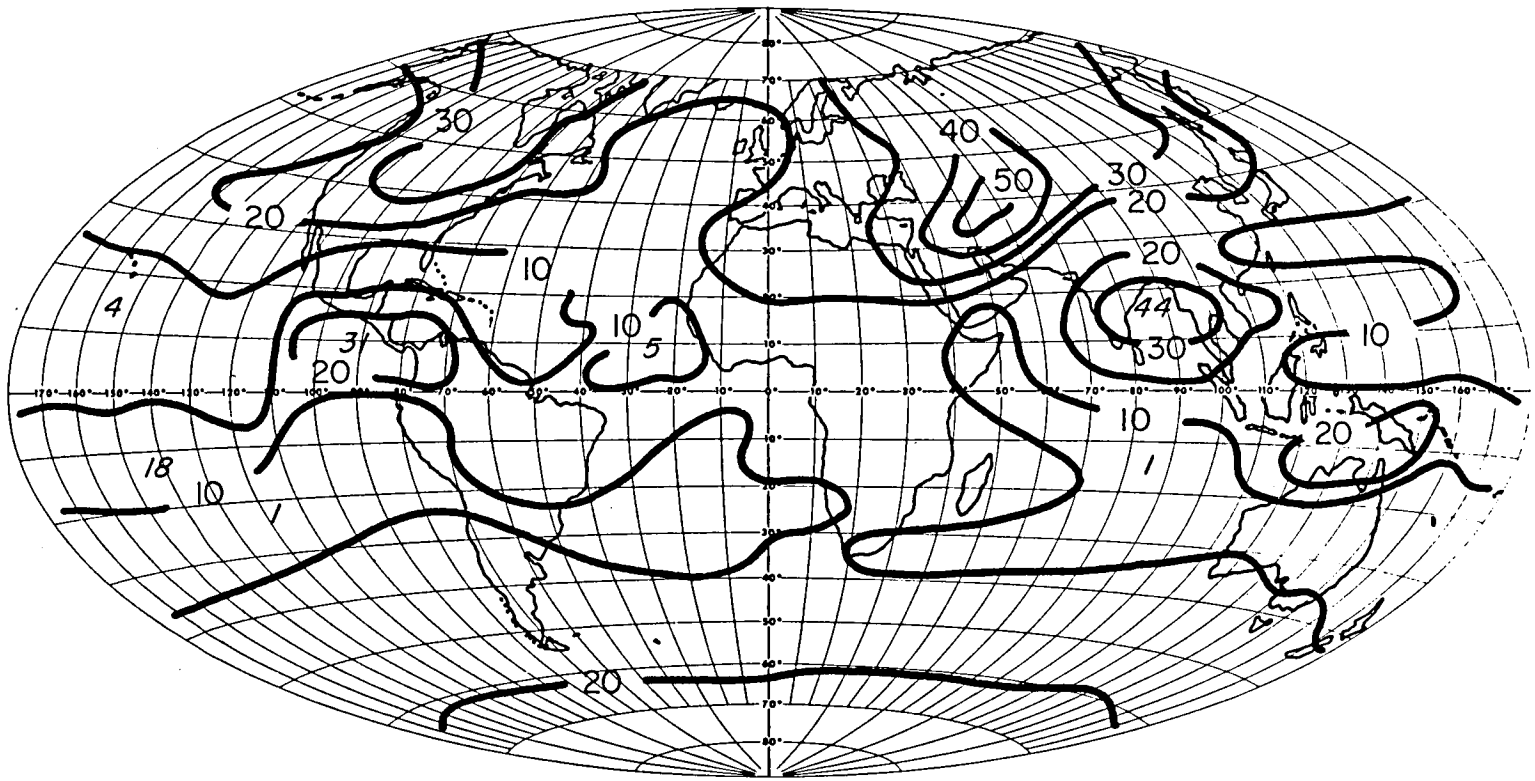
I-AMPLITUDE (W/m²)
ANNUAL
30
20
10
4
3
20
10
5
40
50
30
20
20
44
30
10
10
1
20
18
10
1
20

Fig. 12a

Figs. 12b and c show maps of the explained variance of the emitted flux and planetary albedo by the combined annual and semiannual cycles. These individual budget components show more higher frequency variance than the net flux discussed above. The variance of the emitted flux can largely be described in terms of the annual and semiannual cycles except in lower latitude regions. The unexplained variability of planetary albedo on the other hand, is much larger and is indicative of variations of higher frequency than either the annual or semiannual cycles.

I-EXPLAINED VARIANCE (%)
ANNUAL+SEMI-ANNUAL

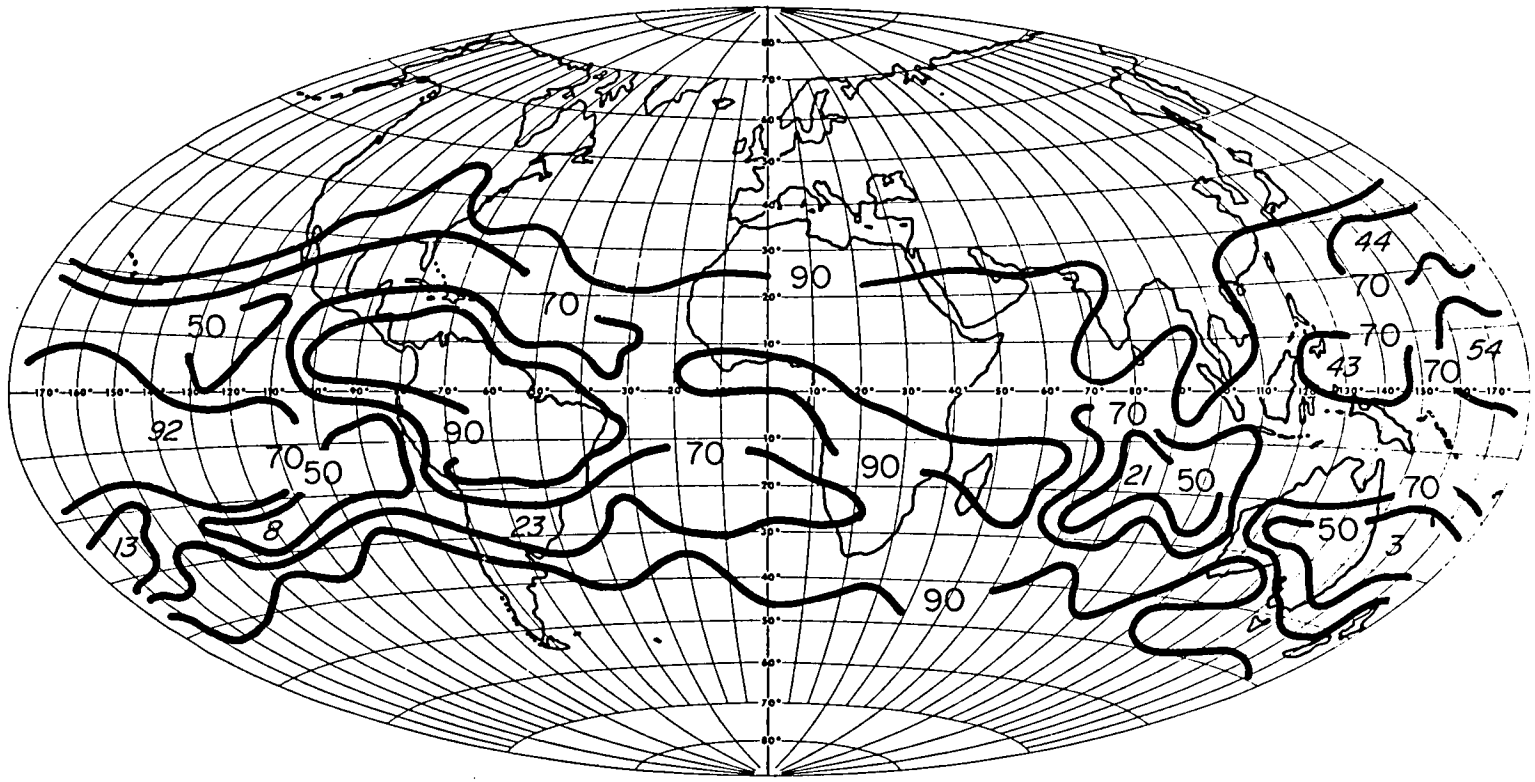

Fig. 12b

α – EXPLAINED VARIANCE (%)

ANNUAL + SEMI-ANNUAL

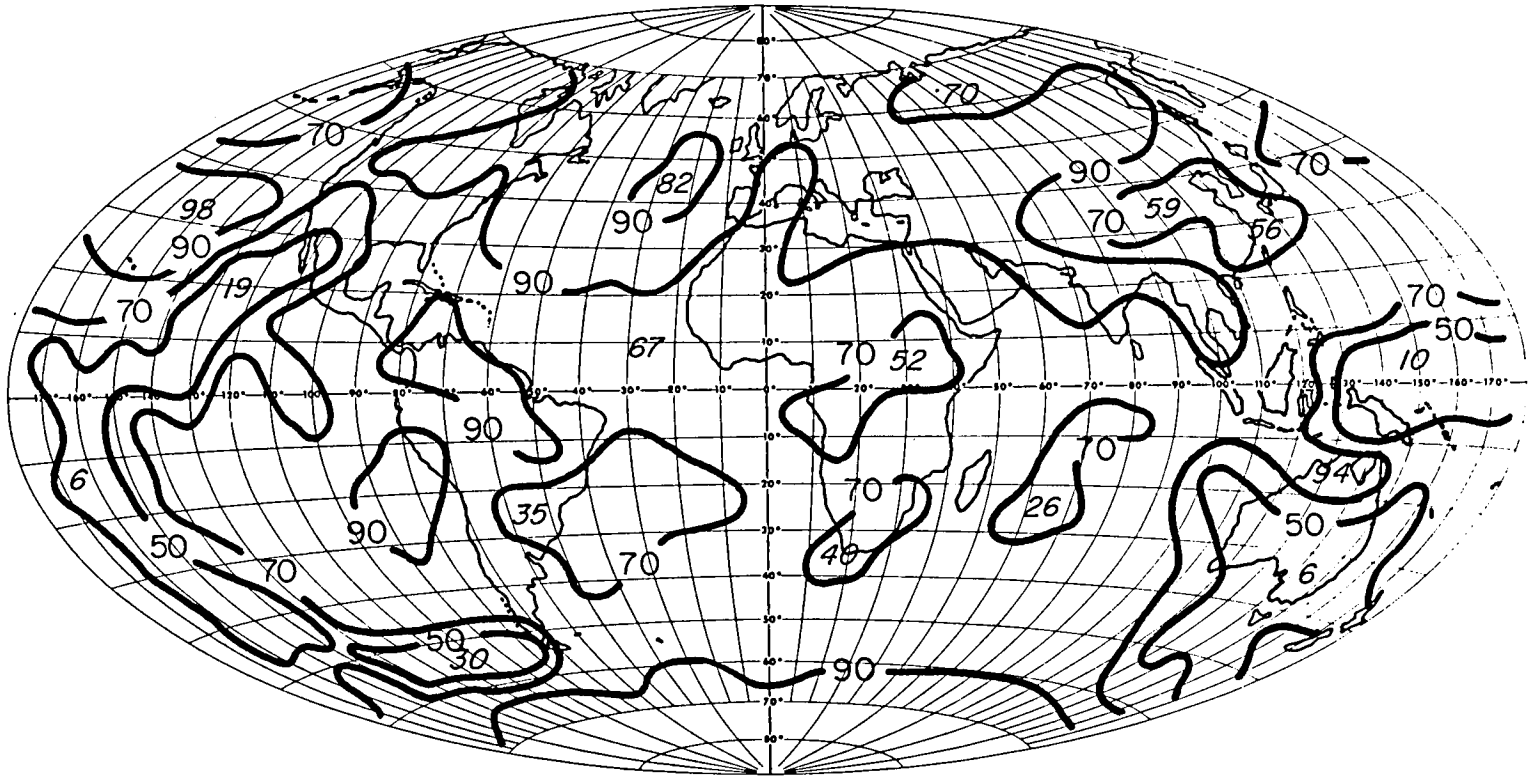

Fig. 12c

4. Model Interpretations of the Radiative Budgets

The determination of the radiative balance at the Earth's surface is essential to atmospheric modelling and prediction from climatic time scales down to those scales for which radiative heating is significant. Further, the radiative budget at the earth's surface is important for the understanding of the partitioning of poleward energy transports into its atmospheric and oceanic components. A radiative transfer model (adapted from Stephens and Webster, 1979) was employed to provide the surface radiative budgets and the budgets determined at the top of the model atmosphere were verified using the satellite data described above. The most satisfactory test of model cloud radiation prescriptions really requires separate measurements of cloud amounts and of solar and infrared fluxes at all levels in the atmosphere. The present test, while less satisfactory is still useful especially if coupled to some measured radiative fluxes at the Earth's surface.

a. Radiative transfer model

The radiative transfer model for the determination of shortwave fluxes within the atmosphere is based largely on the scheme of Stephens and Webster (1979) which incorporates the clear sky parameterizations of Lacis and Hansen (1974). The calculation of the shortwave fluxes within the atmosphere therefore include absorption by water vapour and ozone but none of the smaller absorption by CO_2 and O_2. For this particular study, the Stephens and Webster model is extended to N(=15) layers.

The longwave fluxes from the cloud boundaries (exitances) are determined via the effective emittance approach, i.e.,

$$F^{\uparrow} \text{ (cloud top)} = F_o^{\uparrow} (1-\varepsilon^{\downarrow}) + \varepsilon^{\uparrow} \sigma T_c^4$$

$$F^{\downarrow} \text{ (cloud base)} = F_o^{\downarrow} (1-\varepsilon^{\downarrow}) + \varepsilon^{\downarrow} \sigma T_c^4 \qquad (2)$$

where $F_o^{\downarrow,\uparrow}$ are the respective incident cloud top and base fluxes determined from the radiative transfer equation applicable to the clear sky layers above and below the specified cloud layer, viz

$$F^{\uparrow}(z) = B(T_s)(1 - \varepsilon^{\uparrow}(u)) + \int_o^u B(u')d\varepsilon^{\uparrow}(u')$$

$$F^{\downarrow}(z) = \int_o^u B(u')d\varepsilon^{\downarrow}(u') \qquad (3)$$

where B is the black body function (in flux units) and u is the absorber amount for the path extending from the level of interest (z) to the appropriate boundary (ground, cloud base or top or top of the atmosphere). Note that we have differentiated between upward and downward emittances which were taken from Rodgers (1967) with the correction for the "e type" absorption effect as discussed in Stephens and Webster (1979).

Thus the first term on the right hand side of (2) represents the contribution to the exitance by the transmitted components of the incident flux and the second term is the emitted component by the cloud layer with a temperature T_c. Thus (3) and (2) are coupled together with (3) determining the boundary fluxes at cloud top and base and (2) is applied to determine the exitant fluxes from the cloud.

An atmosphere with multiple cloud layers was treated in the same manner as by Manabe and Strickler (1964). Simply, the flux at some level z above (say) three layers of cloud (high, middle and low) was determined from the combination of radiant fluxes determined for high middle and low cloud separately. The resultant flux becomes

$$F_z^{\uparrow} = F^{\uparrow}_{\text{clear}}(z)\,(1-\theta_l)(1-\theta_m)(1-\theta_h) + \theta_l(1-\theta_m)(1-\theta_h)F^{\uparrow}_{\text{low}} + \theta_m(1-\theta_h)F^{\uparrow}_{\text{mid}} + \theta_h F^{\uparrow}_{\text{high}}(z) \quad (4)$$

where $\theta_{l,m,h}$ are respectively the low, mid and high cloud amounts and the fluxes with subscripts clear, low, mid and high represent those fluxes at reference level z determined for clear sky and overcast sky contitions assuming low, mid and high cloud. A similar expression can be written for the downward fluxes.

A brief outline describing the method of incorporating the transmittance in the radiative transfer model is presented below.

(i) Water vapour transmittance

The transmittance through the major water vapour absorption bands is incorporated in the model using the temperature dependent gray body emissivity approach of Rodgers (1967) with the extension of Stephens and Webster (1979) to include the absorption in the atmospheric window region which is dependent on water vapour partial pressure ("e type" absorption). The absorber amount assumed is corrected for pressure effects by employing the scaled formula

$$u = \int \frac{c(\phi)}{g} P_s \, \phi^{\alpha} \, d\phi \quad (5)$$

where $c(\phi)$ is the water vapour mixing ratio, P_s is the surface pressure, g is the acceleration under gravity, $\phi = P/P_s$ and α is chosen for the suitable absorption band. In this case, $\alpha = 0.9$ for the entire combined water vapour absorption. There is no theoretical justification for the one parameter scaling approach (5) but it is generally recognized that such a correction is better than none at all. Comparison of radiative transfer schemes employing this approach to those employing a higher order correction (the Curtis Godson approximation) show acceptably good agreement at least in the troposphere (Stone and Manabe, 1968). This approach is likely to be reasonable for water vapour absorption in the troposphere but is not acceptable for CO_2 and O_3 absorption in the stratosphere.

(ii) Water vapour - CO_2 overlap (15 μm)

The CO_2 - water vapour overlap region is treated as a single interval 200 cm^{-1} wide centred at 667 cm^{-1} (after Rodgers and Walshaw, 1966). The transmittance employed in the model is determined from the multiplication of the transmittance of each gas via

$$\tau_{CO_2\text{-}H_2O} = \tau_{CO_2} \cdot \tau_{H_2O} \qquad (6)$$

Equation (6) is valid provided the transmittance of each gas is expressed in a suitable form which preserves its multiplicative properties. The statistical band model (exponential in form) is applied to determine both τ_{H_2O} and τ_{CO_2} using the published band model properties of Rodgers and Walshaw (1966).

Correction for pressure variations along the absorption path are performed by application of the Curtis Godson approximation which

defines a scales absorber amount $\bar{u}$ and a mean pressure $\bar{\phi}$ by

$$\bar{u} = \int d\mu$$

$$\bar{u}\ \bar{\phi} = \int \phi d\mu \qquad (7)$$

(iii) Transmission in the 9.6 μm ozone band

Neither the Goody random model (as employed above for the CO_2 - H_2O overlap) nor the Curtis Godson approximation are adequate to describe the absorption of IR radiation by ozone. The latter approximation can introduce substantial error to the transmittance estimates. A simple 3 parameter approximation (c.f. the two parameter Curtis Godson approximation) after Goody (1964) is included in the Malkmus (1967) random model (e.g. Rodgers, 1968). The three parameter approximation is far more simple than that introduced by Kuriyan et al. (1977) and performs equally as well.

(iv) Cloud-radiative properties

The radiative properties of the various cloud types are selected in the following manner. Low and middle level clouds are assumed to be water clouds and their long- and shortwave properties are determined from the parameterization of Stephens (1978b). The shortwave absorption and albedo are similarly estimated from that parameterization for the given solar zenith angles. The radiative properties are so derived for an assumed liquid water path of 140 $g.m.^2$ (i.e., for a cloud with a visible optical thickness of 39).

The reflectance emittance relation assumed in the present model is determined assuming the cloud albedo-liquid water path parameterization of Stephens (1978b) for water clouds. The effective emittance-liquid (ice) water path (W) was adjusted as

$$\varepsilon^{\downarrow,\uparrow} = 1 - \exp(0.1\ W) \qquad (8)$$

for high cloud to make the combined reflectance emittance relation consistent with satellite deduced observations of Platt et al. (1980).

The extent to which (8) is valid is difficult to determine but it does agree well with the results derived from the observations of Cox and Griffith (1979).

b. Zonally averaged data

The following calculations were performed using the zonally averaged fields of temperature and humidity published by Oort and Rasmussen (1971). All other latitude dependent parameters required by the model are shown in Table 2. Most of these data were taken from Ohring and Adler (1978) and the cloud amounts were adopted from Manabe (1969) who based his values on London (1957). The cloud position was also taken from Manabe and the cloud was assumed to exist somewhere in the specified layer.

c. Simulation of zonally averaged radiative fields

In this section, the model calculations of the radiative quantities employing the zonally averaged parameters described above are compared with observations and previous radiative budget calculations. The model radiative sources and sinks are a critical factor for any climate modelling exercise and it should prove interesting to compare the present radiative budget calcuations to past calculations particularly emphasizing discrepancy between the two.

Fig. 13 shows the comparison of the zonally averaged profile of emitted flux, planetary albedo and net flux as computed by the model and deduced from the satellite observations discussed above. Generally, the model calculations and the observed values agree extremely closely. In

Table 2. Summary of latitude dependent parameters

Parameters	0-10	10-20	20-30	30-40	40-50	50-60	60-70	70-80	80-90
Insolation ($W.m^{-2}$)	418	407	371	352	310	263	216	188	176
Mean (daily) cosine of zenith angle	0.609	0.592	0.539	0.512	0.451	0.383	0.314	0.273	0.256
Surface albedo	0.064	0.080	0.106	0.112	0.14	0.157	0.404	0.491	0.65
Cloud amount									
Low	0.317	0.264	0.248	0.302	0.388	0.438	0.444	0.424	0.375
Mid	0.074	0.064	0.063	0.079	0.110	0.131	0.119	0.111	0.092
High	0.225	0.181	0.160	0.181	0.210	0.242	0.254	0.252	0.205
Cloud position									
Low	700 - 900 mb								
Mid	500 - 700 mb								
High	200 - 300 mb								

Fig. 13

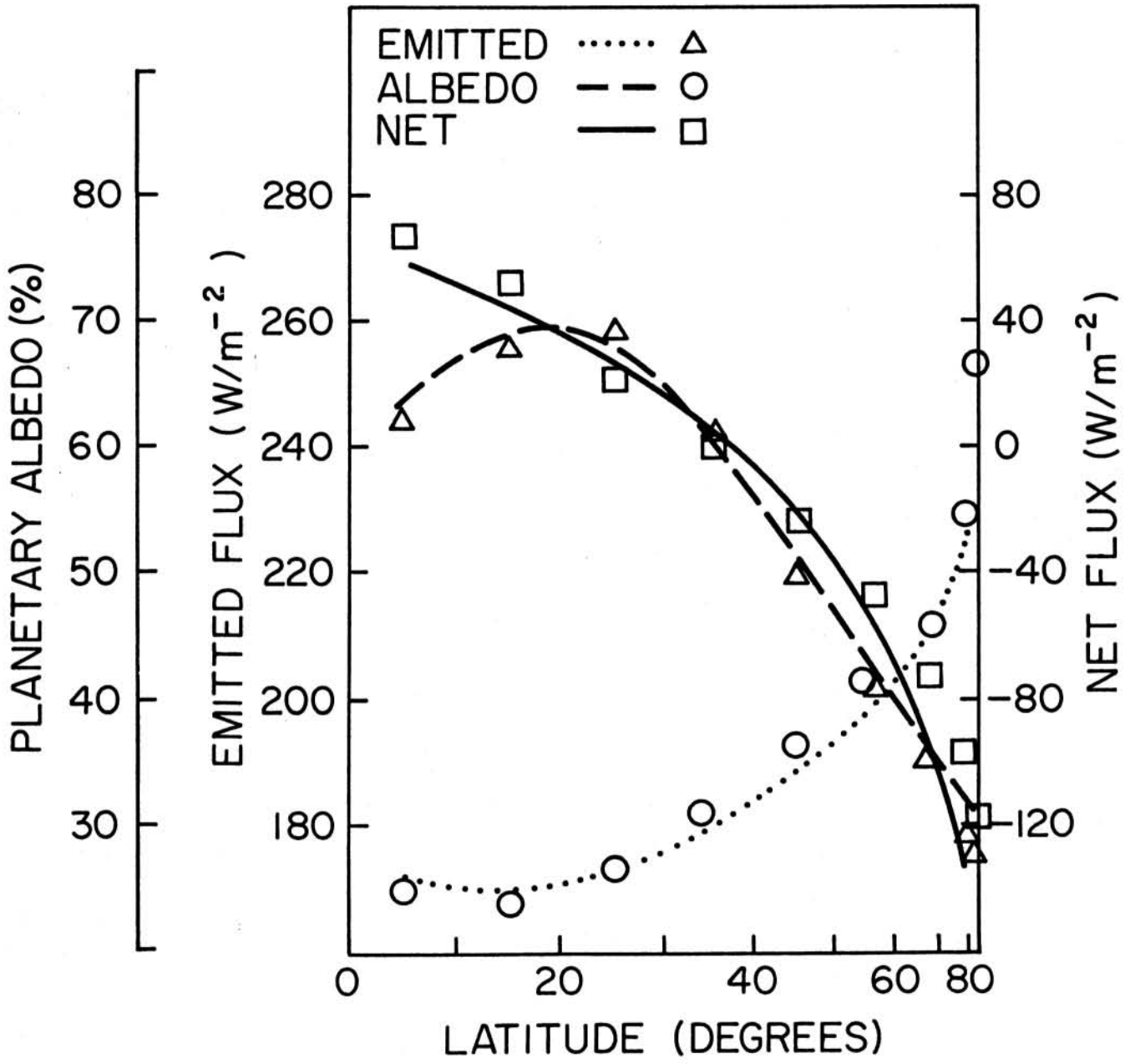
EMITTED
ALBEDO
NET
PLANETARY ALBEDO (%)
EMITTED FLUX (W/m⁻²)
NET FLUX (W/m⁻²)
LATITUDE (DEGREES)
80
70
60
50
40
30
280
260
240
220
200
180
80
40
0
-40
-80
-120
0
20
40
60
80

particular, the variation of the radiation budget components with latitude is well handled, except for the albedo comparison in the polar regions. As mentioned above, the deduced albedos from satellite data require a significant correction for bidirectional reflectance and the values in this region must be viewed with some caution.

Figs. 14 a and b show comparisons of the model calculations with London's (1957) radiative budget calculations of surface absorption of shortwave radiation and net flux of longwave radiation respectively. The shortwave energy absorbed at the earth's surface calculated by the present model is generally larger than those of London. For example, at 15^{o}N the computed solar radiation reflected to space is 26%; absorbed in the atmosphere, 17%, and absorbed in the ocean, 57%. These may be compared to those of London with estimates of 34%, 14%, and 52%. The differences are consistent with the findings of Vonder Haar and Hanson (1969) who found, from observational evidence that the amount of shortwave radiant energy absorbed at the surface in tropical regions is 61% with reflected and absorbed amounts of 24% and 14% respectively.

The net longwave fluxes at the surface as calculated by the present model are significantly smaller in low latitude regions than those of London. The solid bars included on the diagram are the values obtained from measurements during the convectively disturbed (cloudy), and convectively undisturbed (mostly clear) phases of GATE. The dashed horizontal line (all phases) is the value of the net longwave surface flux which is an average between the disturbed and suppressed conditions. These GATE results are averages over the A array (5^{o} - 12^{o}N) and suggest that the net flux of longwave radiation at the surface is fairly invariant over the highly opaque tropical atmosphere. It is therefore possible to

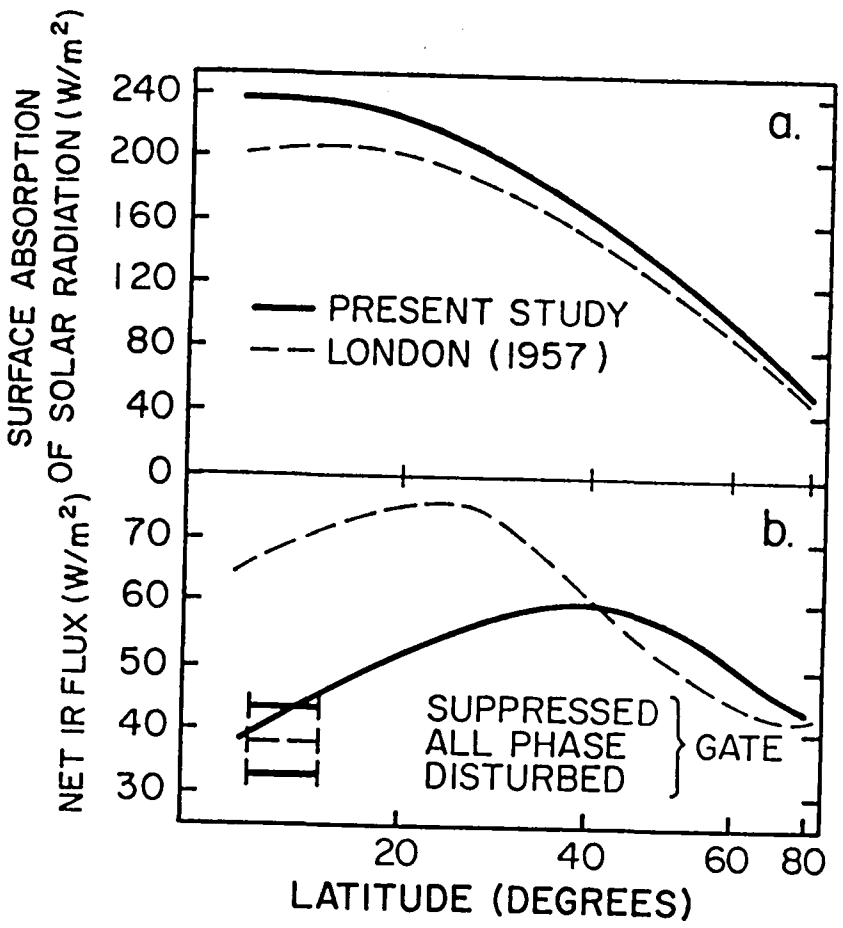
SURFACE ABSORPTION
NET IR FLUX (W/m²) OF SOLAR RADIATION (W/m²)
240
200
160
120
80
40
0
70
60
50
40
30
a.
b.
PRESENT STUDY
LONDON (1957)
SUPPRESSED
ALL PHASE
DISTURBED
GATE
20
40
60
80
LATITUDE (DEGREES)

compare meaningfully the model calculations employing annual mean profiles of moisture and temperature in tropical regions with the measurements from GATE.

The discrepancies that exist between the current model calculations (and observations) to those previously estimate from budget calculations are a direct result of the inclusion of additional absorption in the 8-14 μm window regions by a water vapour partial pressure dependent absorption mechanism. The presence of this absorption has been realized since the early seventies (Bignell, 1970, among others). The effect of including this absorption produces a major increase in longwave cooling rates in the lowest levels of the tropical atmosphere. These changes, which are as large or larger than $2^{\circ}C$/day (Stephens, 1976) agree closely with the observed profile (e.g., Cox, 1969) which first indicated anomalous cooling in the lowest levels of the tropical atmosphere. The comparison presented in Fig. 14b further illustrates such agreement between observation and theoretical calculation. The mechanism for this absorption is still open to debate with favoured explanations relying on the existence of a water dimer molecule (e.g., Montgomery, 1978).

Despite the acceptance of the existence of this enhanced absorption, it has not been fully recognized in meteorological studies (Burrough, 1979). It is evident from Fig. 14b that the resulting increased atmospheric emission supplies significantly more energy to the surface in the tropics than previously estimated. As a result, the excess energy available for transport towards the poles in the oceans or the air-sea interface energy exchange must be larger than hitherto assumed. These considerations are of prime importance for climate studies and numerical models designed to simulate atmospheric circulations must be concerned with including this radiative process.

5. Summary and Conclusions

This paper presents the earth atmosphere radiation budgets derived from satellite observations for both seasonal and annual averages. The budgets are derived from a composite of 48 monthly mean radiation budget maps and represents a continuing compilation first reported by Vonder Haar and Suomi (1971). The broad features presented in this paper for the annual average are similar to those reported earlier. The annual globally averaged emitted flux is 234 $W.m^{-2}$, the planetary albedo is 0.30 and the net flux is zero, at least within measurement uncertainty. Also, the annual and season zonally averaged profiles of net flux show the predictable net energy input to the lower latitudes and net energy loss at higher latitudes thus providing the differential heating between the equator and poles which must be balanced by the attendant poleward transport of heat by the atmosphere and ocean.

Although the analysis of the radiation budget in zonally averaged terms is convenient and customary, such an analysis is not natural particularly when one recognizes the differences of climate imposed by continentality. This influence is apparent in the geographic distribution of planetary albedo in particular. Further, the net flux distribution displays distinct regions of zonal assymetry particularly in those latitudes associated with maximum solar insolation. The most dramatic changes in net flux distribution occur for the transition from solstice to equinox.

The distribution of annual net flux displays different spatial scales in the latitude belt from about $30^{o}N$ and $30^{o}S$. This can be largely attributed to the albedo which is highly influenced by desert regions and the extensive areas of stratocumulus clouds off the west

coasts of South Africa and South and North America. These regions appear as relative minima in net flux and are distinctly evident in the Southern Hemisphere along with the Australian desert.

The globally averaged net flux displays an annual cycle which is mainly attributed to the annual cycle imposed by the externally forcings associated with earth-sun geometry. A study of the geographic distribution of the total variability (defined as the total variance determined from the individual monthly data) of net flux reveals that generally greater than 95% of the variability occurs because of the semi and annual cycles imposed by the regular earth sun geometry variations throughout the year. The individual components of emitted flux and planetary albedo display more high frequency variability particular equatorward of about 30^{o} latitude. In these regions, the spatial and temporal scales of albedo are dominated by cloud free oceans and cloudy and desert area differences and thus the albedo is likely to display some high frequency variability governed by cloud distributions in particular. The variability of emitted flux, on the other hand, is governed by regions of cloud free (including low cloud) and very high cloud, particularly convective cloud zones and as a result is less variable than albedo. Except in regions over deserts and low cloud, these albedos are negatively correlated with emitted flux. This reciprocity is due to the cloud influence on emitted and reflected fluxes and occurs such that the total upwelling flux from the earth atmosphere system remains more or less uniform.

Radiative transfer simulations of the observed budget quantities, at least for the zonally averaged case, are good. Significant differences occur largely as a result of exclusion of enhanced absorption

in the 8-14 μm regions by a proposed water vapour dimer in the earlier calculations. The discrepancy results in some 35 $W.m^{-2}$ more radiant energy into the oceans in the tropics than previously estimated. The validity of this result was verified using results from the GATE radiation budget measurements. As a result, this excess energy input into the oceans in lower latitudes must result in larger poleward heat transports by the oceans or air sea interface energy exchanges.

The results summarized above suggest that it may be difficult and ambiguous to verify the global and zonal radiative transfer calculations of climate models using the satellite derived radiation budget results without consideration of surface conditions. It was shown that the changes of the emitted and reflected fluxes, largely due to cloud distribution variations, often negatively correlate such that the net flux is less sensitive to cloud and the variability of net flux is forced primarily by the semiannual and annual cycles imposed by the regular variation of earth-sun geometry throughout the year. Thus, the net flux, and its variability, can be successfully modelled in general in terms of the rather simple earth-sun geometry requirements and with seasonally invariant cloud cover. However, this may overlook major climate impact areas of poor radiation reciprocity such as land deserts, stratus regimes and cirrus areas. Furthermore, the general treatment does not ensure that either the surface radiation budgets or the atmospheric heating are modelled adequately. It is the latter quantity that provides the only radiative influence on the rest of the model dynamics.

References

Bignell, K. J., The water vapour infrared continuum. Quart. J. R. Met. Soc., 96, 390-403, 1970.

Burroughs, W. J., The water dimer: a meteorologically important molecular species. Weather, 34, 233-236, 1979.

Campbell, G. G. and T. H. Vonder Haar, Climatology of Radiation Budget Measurements from Satellites. Atmos. Sci. Paper, No. 322, Colorado State University, Fort Collins, Colorado, 65 pp., 1980.

Cess, R. D., Climate Change: An appraisal of atmospheric feedback mechanisms employing zonal climatology. J. Atmos. Sci., 33, 1831-1843, 1976.

Charney, J., Dynamics of deserts and droughts in the Sahel. Quart. J. R. Met. Soc., 101, 193-202, 1975.

Cox, S. K., Observational evidence of anomalous infrared cooling in a clear tropical atmosphere. J. Atmos. Sci., 26, 1347-1349, 1969.

Cox, S. K. and K. T. Griffith, Estimates of Radiative Divergence during Phase III of GATE. Part I, Methodology. J. Atmos. Sci., 36, 566-575, 1979.

Ellis, J. S. and T. H. Vonder Haar, Zonal average earth radiation budget measurements from satellites for climate studies. Atmos. Sci. Paper No. 240, Colorado State University, Ft. Collins, Colorado, 50 pp., 1976.

Ellis, J. S., T. H. Vonder Haar, S. Levitus and A. H. Oort, The annual variation in the Global Heat Balance of the Earth. J. Geophys. Res., 84, 1958-1962, 1978.

Goody, R. M., The transmission of radiation through an inhomogeneous atmosphere. J. Atmos. Sci., 21, 575-581, 1964.

Gruber, A. and J. S. Winston, Earth-atmosphere radiative heating based on NOAA scanning radiometer measurements. Bull. Amer. Meteor. Soc., 59, 1570-1573, 1978.

Hartmen, D. L. and D. A. short, On the use of earth radiation budget statistics for studies of clouds and climate. Submitted for publication in J. Atmos. Sci., 1980.

Hickey, J., L. Stowe, H. Jacobowitz, P. Pelegrino, R. Maschoff, A. Arking, J. House, A. Ingersoll and T. H. Vonder Haar, Initial solar irradiance determination from Nimbus 7 cavity radiometer measurements. Submitted to Science, 1980.

Kuriyan, J. G., Shippony and S. K. Mitra, Transmission function for IR radiative transfer in an inhomogeneous atmosphere. Quart. J. Roy. Met. Soc., 103, 511-517, 1977.

Lacis, A. and J. G. Hansen, A parameterization for the absorption of solar radiation in the earth's atmosphere. J. Atmos. Sci., 31, 118-133, 1974.

Lau, N-C., The structure and energetics of transient disturbances in the Northern Hemisphere wintertime circulation. J. Atmos. Sci., 36, 982-995, 1979.

Liou, K. N., A numerical experiment on Chandrasetehar's Discrete-Ordinate Method for Radiative Transfer: Applications to Cloudy and Hazy Atmospheres. J. Atmos. Sci., 30, 1303-1326, 1973.

London, J., A study of the atmospheric heat balance. Final Report Contract No. AF 19(122)-165. College of Engineering Res. Div., New York University, 99 pp., 1957. (NTIS No: PB115626)

McKee, T. and S. K. Cox, Simulated Radiance Patterns for Finite Cubic Clouds. J. Atmos. Sci., Vol. 33, 2014-2020, 1976.

Malkmus, W., Random Lorentz band model with exponential tailed S^{-1} line intensity distribution function. J. Opt. Soc. Am., 57, 323-329, 1967.

Manabe, S., Climate and the ocean circulation: I. The atmospheric circulation and the hydrology of the earth's surface. Mon. Wea. Rev., 97, 739-774, 1969.

Manabe, S., and R. F. Strickler, Thermal equilibrium of an atmosphere with a convective adjustment. J. Atmos. Sci., 21, 361-385, 1964.

Montgomery, G. P., Temperature dependence of infrared absorption of water vapor near 1200 cm^{-1}. Appl. Opt., 17, 2299-2303, 1978.

Ohring, G., The effect of changes in cloud amount on the net radiation at the top of the atmosphere. Submitted for publication, 1980.

Ohring, G. and S. Adler, Some experiments with a zonally averaged climate model. J. Atmos. Sci., 35, 186-205, 1978.

Oort, A. H. and E. M. Rasmussen, Atmospheric Circulation Statistics, NOAA Prof. Pap. 5, 323 pp., 1971.

Oort, A. H. and T. H. Vonder Haar, On the observed annual cycle in the ocean-atmosphere heat balance over the Northern Hemisphere. J. Phys. Ocean., 6, 781-800, 1976.

Platt, C. M. R., D. Reynolds and N. Abshire, Albedo of cirrus-inferences from groundbased lidar and geostationary satellite observations. Submitted to Mon. Wea. Rev., 1980.

Raschke, E. and W. R. Bandeen, The radiation balance of the planet Earth from radiation measurements of the satellite Nimbus 2. J. Appl. Meteor., 9, 215-238, 1970.

Raschke, E., T. H. Vonder Haar, W. R. Bandeen and M. Pasternak, The annual radiation balance of the Earth-Atmosphere system during 1969-70 from Nimbus 3 measurements. J. Atmos. Sci., 30, 341-364, 1973.

Riehl, H. and A. Miller, Differences between morning and evening temperatures of cloud tops over tropical continents and oceans. Quart. J. R. Met. Soc., 104, 757-764, 1978.

Rodgers, C. D., The use of emissivity in atmospheric radiation calculations. Quart. J. Roy. Met. Soc., 93, 45-54, 1967.

Rodgers, C. D., Some extensions and applications of the new random model for molecular band transmission. Quart. J. Roy. Met. Soc., 94, 99-102, 1968.

Rodgers, C. D. and C. D. Walshaw, The computation of infrared cooling rates in planetary atmospheres. Quart. J. Roy. Met. Soc., 92, 67-92, 1966.

Schneider, S. H., Cloudiness as a global feedback mechanism: The effects on the radiation balance and surface temperature variations in cloudiness. J. Atmos. Sci., 29, 1413-1422, 1972.

Short and Wallace, Satellite inferred morning to evening cloudiness changes. Submitted to Mon. Wea. Rev., 1980.

Stephens, G. L., An improved estimate of IR cooling in the atmospheric window region. J. Atmos. Sci., 33, 806-809, 1976.

Stephens, G. L., Radiative properties of extended water clouds II. Parameterizations. J. Atmos. Sci., 2123-2132, 1978.

Stephens, G. L., Radiative transfer on a linear lattice: Application to anisotropic ice crystal clouds. Submitted to J. Atmos. Sci., 1980.

Stephens, G. L. and P. J. Webster, Sensitivity of radiative forcing to variable cloud and moisture. J. Atmos. Sci., 36, 1542-1556, 1979.

Stone, H. M. and S. Manabe, Comparison among various numerical models designed for computing infrared cooling. Mon. Wea. Rev., 96, 735-741, 1968.

Vonder Haar, T. H. and J. Hansen, Absorption of solar radiation in tropical regions. J. Atmos. Sci., 26, 652-655, 1969.

Vonder Haar, T. H. and V. Suomi, Measurements of the Earth's radiation budget from satellites during a 5 year period. Part I: Extended time and space means. J. Atmos. Sci., 28, 305-314, 1971.

Welch, R. M., S. K. Cox and J. Davis, Solar radiation and clouds. Meteorological Monographs, 39, 1980.

Winston, J. S., Planetary scale characteristics of monthly mean longwave radiation and albedo and some year to year variations. Mon. Wea. Rev., 95, 235-256, 1967.

1. Report No. NASA CR-159232	2. Government Accession No.	3. Recipient's Catalog No.
4. Title and Subtitle EARTH RADIATION BUDGET MEASUREMENTS FROM SATELLITES AND THEIR INTERPRETATION FOR CLIMATE MODELING AND STUDIES		5. Report Date 6. Performing Organization Code
7. Author(s) G. L. STEPHENS, T. H. VONDER HAAR, & G. G. CAMPBELL		8. Performing Organization Report No. 10. Work Unit No.
9. Performing Organization Name and Address Department of Atmospheric Science Colorado State University Fort Collins, CO 80523 USA		11. Contract or Grant No. 13. Type of Report and Period Covered
12. Sponsoring Agency Name and Address NASA Langley Research Center Hampton, VA 23665		14. Sponsoring Agency Code

15. Supplementary Notes

16. Abstract

The report presents the annual and seasonal averaged earth atmosphere radiation budgets derived from the most complete set of satellite observations available in late 1979. The budgets were derived from a composite of 48 monthly mean radiation budget maps. Annually and seasonally averaged radiation budgets were presented as global averages, zonal averages. Also, the geographic distribution of the various radiation budget quantities were presented. The annual cycle of the radiation budget was analyzed and the annual variability of net flux was shown to be largely dominated by the regular semi and annual cycles forced by external earth-sun geometry variations. Radiative transfer calculations were compared to the observed budget quantities and surface budgets were additionally computed with particular emphasis on discrepancies that exist between the present computations and previous surface budget estimates.

17. Key Words (Suggested by Author(s))	18. Distribution Statement
Radiation budgets of earth Climatology of radiation budgets Satellite measurements of radiation budgets	Unclassified - unlimited

19. Security Classif. (of this report)	20. Security Classif. (of this page)	21. No. of Pages	22. Price*
Unclassified	Unclassified	57	

N-305

For sale by the National Technical Information Service, Springfield, Virginia 22161